J. Fluid Mech. (2006), *vol.* 557, *pp.* 423–450. © 2006 Cambridge University Press
doi:10.1017/S0022112006009906 Printed in the United Kingdom

Effects of unsteady blowing through a spanwise slot on a turbulent boundary layer

By KYOUNGYOUN KIM AND HYUNG JIN SUNG†

Department of Mechanical Engineering, Korea Advanced Institute of Science and Technology, 373-1 Guseong-dong, Yusong-gu, Daejeon, 305-701, Korea

(Received 6 April 2005 and in revised form 1 December 2005)

The effects of localized periodic blowing on a turbulent boundary layer were investigated by direct numerical simulation. Time-periodic blowing was applied through a spanwise slot by varying the wall-normal velocity in a cyclic manner from 0 to $2A^+$. Time-periodic blowing was applied at frequencies in the range $0 \leqslant f^+ \leqslant 0.08$ at a fixed blowing amplitude of $A^+ = 0.5$. Simulations of a spatially evolving turbulent boundary layer were carried out for two Reynolds numbers, $Re_{\theta,in} = 300$ and 670. Before investigating the effects of periodic blowing, the effects of steady blowing were examined. A new parameter, σ^+, was proposed for describing local blowing; the usefulness of this parameter was that the responses of the flow variables at the two Reynolds numbers were the same for the same σ^+. The effects of varying the blowing frequency were scrutinized by examining the phase- or time-averaged turbulent statistics. For both Reynolds numbers, application of blowing at a frequency of $f^+ = 0.035$ was found to give the maximum increases in Reynolds shear stress, streamwise vorticity fluctuations and energy redistribution. Analysis of the Reynolds stress budget showed that this effective blowing frequency induced the greatest enhancement of the pressure–strain term, which is closely related to the energy redistribution. Analysis of the phase-averaged stretching and tilting terms revealed that the stretching term is significantly enhanced in the 'downward' motion that is induced by the spanwise vortical motion. The correlation between the streamwise vorticity and the stretching term changed in magnitude and length scale as the blowing phase was varied, whereas the correlation between the streamwise vorticity and the tilting term did not.

1. Introduction

Advances in the understanding of the coherent structure of wall-bounded turbulent flow have intensified interest in controlling near-wall turbulence. Many attempts have been made to devise a practical method for controlling wall-bounded flows. These include the modification of the wall surface by installing riblets (Choi, Moin & Kim 1993), as well as the use of a compliant wall (Choi *et al.* 1997), wall deformations (Kim *et al.* 2003*a*) or a spanwise oscillating wall (Choi, Xu & Sung 2002). These are discussed in Gad-el-Hak (2000). Among the approaches considered to date, the use of local suction/blowing deserves more detailed study because it provides an efficient and simple means for locally actuating the wall-bounded flow. Moreover, the strength of the actuation can be controlled with relative ease by local suction/blowing. Many

† Author to whom correspondence should be addressed. hjsung@kaist.ac.kr.

engineering applications use local forcing to modify a turbulent boundary layer. For example, local blowing is widely used to protect surfaces from high temperatures in gas turbines and to cool electronic chips.

Most previous experimental and numerical studies of local suction/blowing have focused on steady actuation (Sano & Hirayama 1985; Park & Choi 1999; Krogstad & Kourakine 2000; Kim, Sung & Chung 2002*b*). It is reported that local steady blowing shifts near-wall streamwise vortices away from the wall, thereby reducing the interaction of the vortices with the wall. Steady blowing leads to a reduction in the skin friction near the wall, combined with an increase in the turbulence intensity and skin friction far downstream from the slot. In contrast to the numerous studies that have considered steady blowing, relatively few experimental or numerical studies have examined unsteady suction/blowing (Tardu 1998, 2001; Park, Lee & Sung 2001; Rhee & Sung 2001; Park, Park & Sung 2003). Park *et al.* (2001) performed experiments to probe the effects of periodic blowing and suction through a spanwise slot on a turbulent boundary layer. They found that higher forcing frequencies induced greater changes in the turbulent structures of the boundary layer in their system. In a study of local oscillating blowing, Tardu (2001) found that when the blowing frequency exceeded a critical value ($f^+ = f\nu/u_\tau^2 = 0.008$, where ν is the kinematic viscosity and u_τ is the friction velocity), blowing induced a positive wall vorticity layer that subsequently rolled up into a coherent spanwise vortex. However, the above studies on unsteady forcing employed very large-amplitude forcings ($30 \sim 40$ % of the free-stream velocity), which change the flow significantly, and hence they focused on the evolution of a newly generated strong spanwise vortical structure due to the large-amplitude forcing rather than on the response of the near-wall coherent structure. Kim & Sung (2003) investigated the effects of localized time-periodic blowing by carrying out direct numerical simulations for three cases of relatively small blowing amplitude (less than 5 % of the free-stream velocity). They found that the energy redistribution is enhanced by periodic blowing. Although it is expected that the turbulence structure will be more sensitive to the blowing frequency than the blowing strength, they dealt with only a single blowing frequency ($f^+ = 0.017$).

Near-wall streamwise vortices are known to play a dominant role in wall-bounded flows (Robinson 1991); however, the frequency responses of such vortices to unsteady periodic blowing have not been studied in detail. In the present work, the effect of blowing frequency on the flow characteristics of a turbulent boundary layer was studied, with particular emphasis on the near-wall turbulent-flow structures downstream of the spanwise slot. Direct numerical simulations were carried out at two Reynolds numbers, $Re_{\theta,in} = 300$ and 670, based on the momentum thickness and free-stream velocity. The slot width was approximately 100 in wall units and localized time-periodic blowing was applied by changing the wall-normal velocity on the spanwise slot. The blowing frequency was varied in a range of $0 \leqslant f^+ \leqslant 0.08$ at a fixed blowing amplitude ($A^+ = A/u_\tau = 0.5$, where A is the blowing amplitude). Before investigating the frequency effect, the effects of steady blowing were examined and a new parameter for localized blowing was formulated. The frequency responses were scrutinized by examining the phase- or time-averaged turbulent statistics. A blowing frequency of $f^+ = 0.035$ gave the greatest increases in Reynolds shear stress, streamwise vorticity fluctuations and energy redistribution compared to the system without the local blowing. Reynolds stress budget analysis revealed that this effective blowing frequency also gave the greatest enhancement of the pressure–strain term. The phase-averaged stretching and tilting terms were analysed to clarify the increase in streamwise vorticity fluctuations. Finally, the correlation coefficients between the streamwise vorticity,

stretching and tilting terms were calculated to generate a quantitative description of the response of the turbulent coherent structures to periodic blowing.

2. Numerical method

For an incompressible flow, the non-dimensional governing equations are

$$\frac{\partial u_i}{\partial t} + \frac{\partial}{\partial x_j} u_i u_j = -\frac{\partial p}{\partial x_i} + \frac{1}{Re}\frac{\partial}{\partial x_j}\frac{\partial u_i}{\partial x_j} \qquad (i = 1, 2, 3), \tag{1}$$

$$\frac{\partial u_i}{\partial x_i} = 0, \tag{2}$$

where x_i are the Cartesian coordinates and u_i are the corresponding velocity components. The free-stream velocity U_∞ and the momentum thickness at the inlet θ_{in} are used for non-dimensionalization. The Reynolds number is defined as $Re = U_\infty \theta_{in}/\nu$, where ν is the kinematic viscosity.

The governing equations (1) and (2) are integrated in time by using the fully implicit decoupling method proposed by Kim *et al.* (2002*a*). All terms are advanced with the Crank–Nicolson method in time, and they are resolved with the second-order central-difference scheme in space. Based on a block LU decomposition, both velocity–pressure decoupling and additional decoupling of the intermediate velocity components are achieved in conjunction with the approximate factorization. The overall accuracy in time is second-order without any modification of boundary conditions. Since the decoupled momentum equations are solved without iteration, the computation time is reduced significantly.

An approximate velocity–pressure decoupling of equations (1) and (2) is made in the series of operations:

$$\boldsymbol{A}\boldsymbol{u}^* = \boldsymbol{r} + \boldsymbol{mbc}, \tag{3}$$

$$\Delta t \boldsymbol{D}\boldsymbol{G}\delta p = \boldsymbol{D}\boldsymbol{u}^* - cbc, \tag{4}$$

$$\boldsymbol{u}^{n+1} = \boldsymbol{u}^* - \Delta t \boldsymbol{G}\delta p, \tag{5}$$

where

$$\boldsymbol{A} = \frac{1}{\Delta t}\left[\boldsymbol{I} + \Delta t\left(\boldsymbol{N} - \frac{1}{2Re}\boldsymbol{L}\right)\right],$$

$$\boldsymbol{r} = \frac{1}{\Delta t}\boldsymbol{u}^n - \boldsymbol{G}p^{n-1/2} + \frac{1}{2Re}\boldsymbol{L}\boldsymbol{u}^n,$$

$$\delta p = p^{n+1/2} - p^{n-1/2}.$$

Here, $\boldsymbol{L}$ represents the discrete Laplacian viscous operator, $\boldsymbol{N}$ is the linear discrete convective operator, $\boldsymbol{G}$ is the discrete gradient operator, $\boldsymbol{D}$ is the discrete divergence operator, Δt is the time increment, and the superscript n denotes the nth time step. The known velocities at the boundary have been imposed on $\boldsymbol{mbc}$ and cbc.

Next, the aforementioned approximate factorization is further extended to the velocity components $\boldsymbol{u}^*$ in equation (3) by using the delta form $\delta\boldsymbol{u}^* = \boldsymbol{u}^* - \boldsymbol{u}^n$. Equation (3) is rewritten as,

$$\boldsymbol{A}\delta\boldsymbol{u}^* = -\boldsymbol{A}\boldsymbol{u}^n + \boldsymbol{r} + \boldsymbol{mbc} \equiv \boldsymbol{R}. \tag{6}$$

Here, the intermediate terms $\delta\boldsymbol{u}^*$ can be calculated separately in the following steps, which are equivalent to equation (6) with second-order accuracy in time by introducing

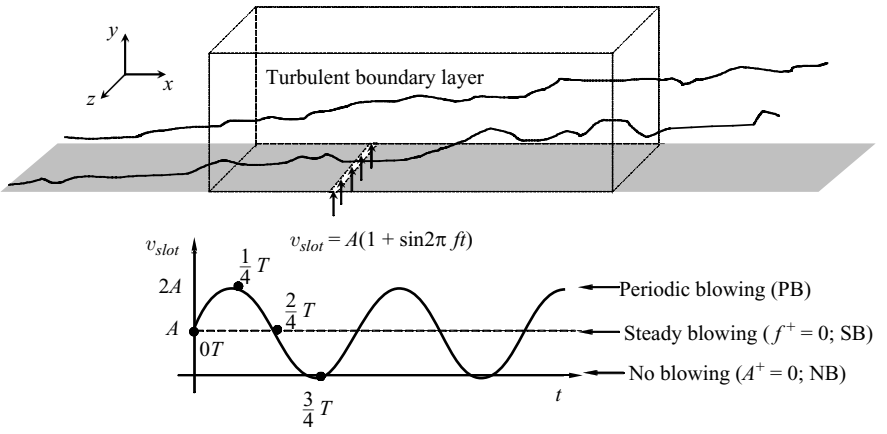

FIGURE 1. Schematic diagram of computational domain.

new variables δu_1^{**} and δu_2^{**}:

$$\frac{1}{\Delta t}(I + \Delta t M_{11})\delta u_1^{**} = R_1, \tag{7}$$

$$\frac{1}{\Delta t}(I + \Delta t M_{22})\delta u_2^{**} = R_2 - M_{21}\delta u_1^{**}, \tag{8}$$

$$\frac{1}{\Delta t}(I + \Delta t M_{33})\delta u_3^{*} = R_3 - M_{31}\delta u_1^{**} - M_{32}\delta u_2^{**}, \tag{9}$$

$$\delta u_2^{*} = \delta u_2^{**} - \Delta t M_{23}\delta u_3^{*}, \tag{10}$$

$$\delta u_1^{*} = \delta u_1^{**} - \Delta t M_{12}\delta u_2^{*} - \Delta t M_{13}\delta u_3^{*}, \tag{11}$$

$$u_i^{*} = u_i^{n} + \delta u_i^{*} \qquad (i = 1, 2, 3), \tag{12}$$

where

$$\boldsymbol{M} = \boldsymbol{N} - \frac{1}{2Re}\boldsymbol{L}.$$

A significant reduction in computing cost and memory is achieved by avoiding the direct inversion of the large sparse matrix $\boldsymbol{A}$. The overall numerical procedure is as follows:

1. Solve $\boldsymbol{u}^*$ from equations (7)–(12) through the velocity decoupling procedure.
2. Solve δp from equation (4).
3. Obtain $\boldsymbol{u}^{n+1}$ from equation (5), which is a divergence-free vector field, and then one time-step marching is finished.

Direct numerical simulations of a turbulent boundary layer for two Reynolds numbers, $Re_{\theta,in} = 300$ and 670, were performed to probe the flow. A schematic diagram of the computational domain is shown in figure 1. The domain size and mesh resolution for the present direct numerical simulations (DNSs) are summarized in table 1. Realistic velocity fluctuations at the inlet are provided based on the method of Lund, Wu & Squires (1998). An auxiliary simulation of the spatially developing turbulent boundary layer was carried out separately to obtain the inflow data. The stored instantaneous plane data of velocity in the inflow simulation are provided at the inlet of the main simulation per each time step. The convective outflow condition $\partial u_i/\partial t + c\partial u_i/\partial x = 0$ is used at the exit, where c is taken to be the mean exit velocity. A no-slip boundary condition is imposed at the solid wall. At the free stream, the

$Re_{\theta,in}$	Lx/θ_{in}	Ly/θ_{in}	Lz/θ_{in}	Lx^+	Lz^+	(Nx, Ny, Nz)	Δx^+	Δz^+	Δy^+_{min}	Δt^+
300	200	30	40	3151	630	(257, 65, 129)	12.3	4.92	0.17	0.248
670	150	30	35	4941	1135	(393, 65, 187)	12.6	5.88	0.20	0.243

TABLE 1. Domain size and mesh resolutions.

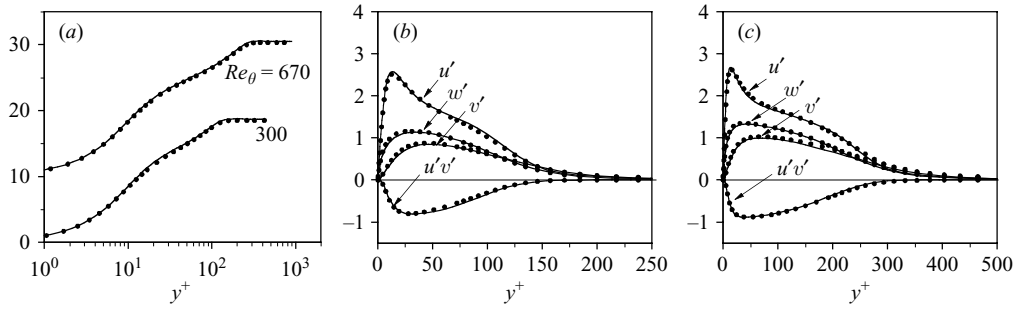

FIGURE 2. Comparison of mean velocity and turbulent intensities. (*a*) U^+; (*b*) Reynolds stresses ($Re_\theta = 300$); (*c*) Reynolds stresses ($Re_\theta = 670$). —, present results; ●, Spalart (1988).

conditions $u = U_\infty$ and $\partial v/\partial y = \partial w/\partial y = 0$ are imposed. Periodic boundary conditions are used in the spanwise direction.

To ascertain the reliability and accuracy of the present numerical simulation, comparisons of the turbulence statistics with the DNS data of Spalart (1988) are made and presented in figure 2. The mean velocity profile normalized by the friction velocity is shown in figure 2(*a*) by $y^+ = yu_\tau/\nu$ and $U^+ = U/u_\tau$. Comparisons are extended to the turbulence intensities and Reynolds shear stress in figures 2(*b*) and 2(*c*). The present results are in excellent agreement with the DNS data at both Reynolds numbers, $Re_{\theta,in} = 300$ and 670. This suggests that the resolution of the present study is sufficient to analyse the second-order turbulence statistics.

The streamwise width of the spanwise slot for localized blowing is $b^+ \approx 100$ in wall units, which is comparable to the width used by Park & Choi (1999). It has been reported that high skin-friction regions on the wall are strongly correlated with near-wall streamwise vortices and the longitudinal length of highly correlated vortices is approximately 100 wall units (Kravchenko, Choi & Moin 1993). The periodic blowing at the slot is generated by varying the wall-normal velocity according to the equation:

$$v_{slot} = A(1 + \sin 2\pi f t). \tag{13}$$

The maximum blowing velocity ($v_{slot} = 2A$) is imparted at $t = 1/4T$ and the minimum ($v_{slot} = 0$) at $t = 3/4T$, where T is the blowing period. At $t = 0/4T$ and $2/4T$, the blowing velocities are the same as those of steady blowing with accelerating and decelerating phases, respectively. The amplitude of the periodic blowing is $A^+ = 0.5$ in wall units, which corresponds to the value of v_{rms} at $y^+ = 15$ without blowing. Here, $A^+ = A/u_{\tau,in}$ and $u_{\tau,in}$ is the friction velocity at the inlet. Hammond, Bewley & Moin (1998) showed that this relatively small actuation significantly affects the turbulent structure in the opposition control of turbulent channel flow. The blowing frequency ($f^+ = f\nu/u^2_{\tau,in}$) varies in the range $0 \leqslant f^+ \leqslant 0.08$. Note that $f^+ = 0$ denotes steady blowing ($v_{slot} = A$). Details regarding the localized blowing conditions are summarized in table 2.

$Re_{\theta,in}$	x_{slot}	b/θ_{in}	b^+	A^+	$\frac{A}{U_\infty}$	$\bar{\sigma}\left(=\frac{\bar{v}_{slot}b}{U_\infty\theta_{slot}}\right)$	$\bar{\sigma}^+ (=\bar{v}^+_{slot}b^+)$	$f^+\left(=\frac{f\nu}{u^2_{\tau,in}}\right)$	$\frac{f\theta_{in}}{U_\infty}$
300	79	6.25	98.5	0.5	0.0263	0.14	50	$0\sim0.08$	$0\sim0.066$
670	75	3.06	101	0.5	0.0246	0.064	50	$0\sim0.08$	$0\sim0.130$

TABLE 2. Localized blowing conditions.

The imposition of periodic blowing may lead to periodic variations in the global physical quantities of the flow. Hence, it is necessary to represent each flow quantity as a superposition of three components

$$q(x, y, z, t) = \bar{q}(x, y) + \tilde{q}(x, y, t/T) + q'(x, y, z, t), \tag{14}$$

where the instantaneous quantity q is decomposed into a time-mean component $\bar{q}$, an oscillating component $\tilde{q}$, and a random fluctuating component q'. The time-average is

$$\bar{q}(x, y) = \frac{1}{T_{tot}L_z}\int_0^{T_{tot}}\int_0^{L_z} q(x, y, z, t)\,\mathrm{d}z\,\mathrm{d}t, \tag{15}$$

where $T_{tot}(=NT)$ is the time over which the quantity is averaged and N is the total number of periods. The oscillating component $\tilde{q}$ is obtained from the relation

$$\tilde{q}(x, y, t/T) = \langle q\rangle(x, y, t/T) - \bar{q}(x, y), \tag{16}$$

where $\langle q\rangle(x, y, t/T)$ is the phase-average, which is defined as

$$\langle q\rangle(x, y, t/T) = \frac{1}{NL_z}\sum_{n=1}^{N}\int_0^{L_z} q(x, y, z, t + nT)\,\mathrm{d}z. \tag{17}$$

Accordingly, the random fluctuation component q' is expressed as

$$q'(x, y, z, t) = q(x, y, z, t) - \langle q\rangle(x, y, t/T), \tag{18}$$

and it follows that $\langle q'^2\rangle = \langle q^2\rangle - \langle q\rangle^2$ and $\langle q'\rangle = \bar{\tilde{q}} = 0$.

3. Localized steady blowing

Before investigating the effect of blowing frequency on a turbulent boundary layer, it is helpful to examine first the effect of steady blowing. Figure 3 shows the streamwise distributions of the skin friction coefficient, pressure coefficient, r.m.s. wall pressure fluctuations and maximum value of the Reynolds shear stress for two Reynolds numbers, $Re_{\theta,in} = 300$ and 670. To validate the grid resolution over the slot, we performed a local steady blowing simulation for $Re = 670$ with doubled streamwise grid points ($N_x = 785$), which allocates 16 grid points over the slot. Note that 8 grid points are located over the slot in the original simulation ($N_x = 393$). The simulation data for two cases are shown in figure 3, where the flow quantity variations with the finer mesh ($N_x = 785$) are almost the same as those with the original one ($N_x = 393$). This suggests that the present grid resolution is enough to resolve the turbulent statistics for localized blowing as well as the unperturbed case (figure 2).

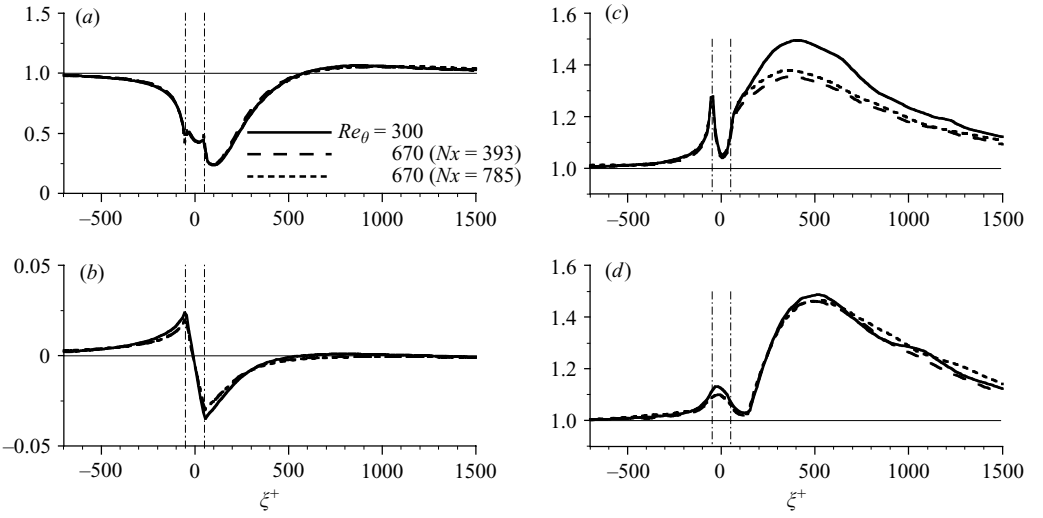

FIGURE 3. Variation of flow quantities in the streamwise direction owing to localized steady blowing ($A^+ = 0.5$, $b^+ = 100$). Here, subscript 'o' denotes no blowing case and $\xi^+ = (x - x_{slot})u_{\tau,in}/\nu$. (*a*) $c_f/(c_f)_o$; (*b*) $c_p/2$; (*c*) $p'_{w,rms}/(p'_{w,rms})_o$; (*d*) $uv_{max}/(uv_{max})_o$.

As shown in figure 3(*a*), C_f decreases rapidly near the slot and increases on moving further downstream. However, the reduction in skin friction near the slot is accompanied by a slight increase in the skin friction downstream of the slot owing to a blowing-induced increase in the turbulence. An adverse pressure gradient is observed upstream and downstream of the slot, whereas a favourable pressure gradient occurs above the slot (figure 3*b*). The overall characteristics of the mean wall variables are in good agreement with previous results (Park & Choi 1999; Kim *et al.* 2002*b*). The r.m.s. wall pressure fluctuations (figure 3*c*) and maximum of the Reynolds shear stress (figure 3*d*) significantly increase downstream of the slot. Considering that high-amplitude wall pressure fluctuations are linked with streamwise vortices and turbulent kinetic energy production, the increase in $p'_{w,rms}$ downstream of the slot may be caused by the activated streamwise vortices and turbulent fluctuations induced by the wall blowing. The similarity of the responses of $p'_{w,rms}$ and $|u'v'|_{max}$ in the downstream suggests that, as was found previously for a turbulent boundary layer with an adverse pressure gradient and separation (Na & Moin 1998), the local maximum Reynolds shear stress may be a good quantity for normalizing wall pressure fluctuations in a locally forced turbulent boundary layer.

Previous studies on systems with localized blowing or suction have employed the parameter σ as a principal parameter to define the local blowing or suction rate:

$$\sigma = \frac{v_{slot} b}{U_\infty \theta_{slot}}, \tag{19}$$

where v_{slot} is the blowing velocity, b is the streamwise width of the spanwise slot, and θ_{slot} is the momentum thickness of the unperturbed flow at the slot location. Thus, σ represents the blowing-induced gain in the momentum flux of the incoming boundary layer. In the present study, $\sigma^+ (= v^+_{slot} b^+) = 50$ was chosen for both $Re_{\theta,in} = 300$ and 670, while the value normalized by outer variables (U_∞ and θ_{slot}) is $\sigma = 0.14$ for

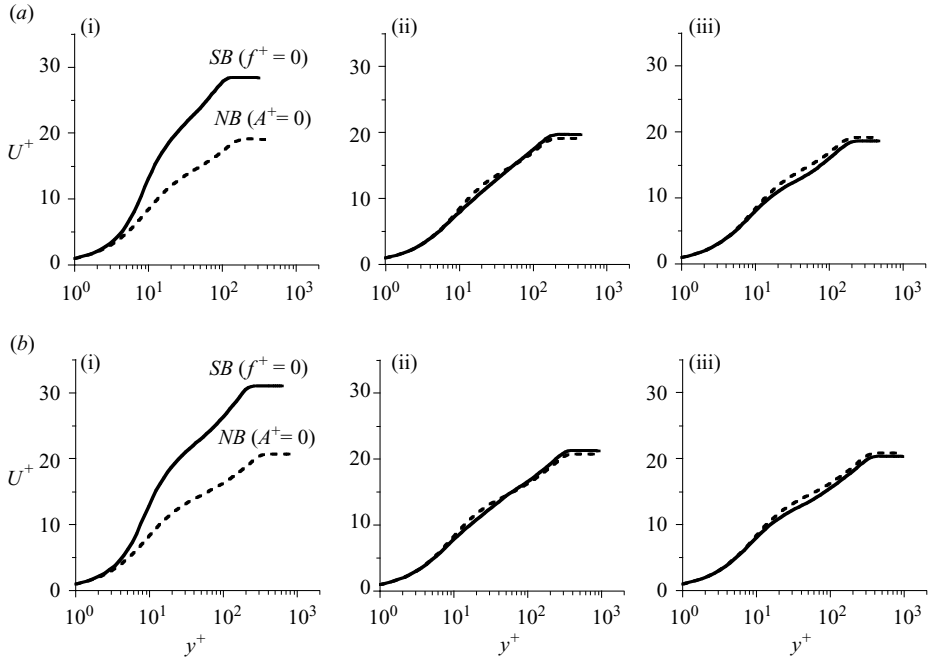

FIGURE 4. Mean velocity profiles in wall coordinates. Here, $y^+ = yu_\tau/\nu$ and u_τ is the local wall-shear velocity. (*a*) $Re_\theta = 300$; (*b*) 670. (i) $\xi^+ = 0$; (ii) 500; (iii) 1000.

$Re_{\theta,in} = 300$ and $\sigma = 0.064$ for $Re_{\theta,in} = 670$. Note that σ^+ can be written as

$$\sigma^+ = v_{slot}^+ b^+ = \frac{v_{slot}}{u_\tau}\frac{bu_\tau}{\nu} = \left(\frac{v_{slot}b}{U_\infty \theta_{slot}}\right)\left(\frac{U_\infty \theta_{slot}}{\nu}\right) = \sigma Re_{\theta,slot}, \tag{20}$$

which reflects the Reynolds-number effect. In figure 3, where the streamwise distance from the centre of the slot is normalized by the viscous length scale (ν/u_τ), the downstream evolution of C_f, C_p and $|u'v'|_{max}$ is almost the same for the two Reynolds numbers. The magnitude of the increase in $p'_{w,rms}$ differs slightly between the two Re values; however, the streamwise location of the maximum increase in $p'_{w,rms}$ is almost the same for the two Re values ($\xi^+ = 400$). The similarity of the responses of the flow variables for the same σ^+ implies that σ^+ can be used as a parameter for defining local blowing on a low-Reynolds-number turbulent boundary layer. However, the normalization of the evolution distance (ξ^+) by the viscous length scale suggests that the forcing is given at a low amplitude and the use of σ^+ is limited.

The mean velocity profiles for the $Re_{\theta,in} = 300$ and 670 systems with steady blowing (SB) are shown in figure 4. For reference, the velocity profiles with no-blowing (NB) are also drawn. For both Reynolds numbers, the velocity profiles of steady blowing show upward shifts above the slot and downward shifts in the downstream. This behaviour is consistent with the results of Park & Choi (1999). These upward and downward shifts are related to the decrease and increase in skin friction induced by the local blowing shown in figure 3(*a*). Furthermore, the spatial evolution of the velocity profile for $Re_{\theta,in} = 300$ is similar to that for $Re_{\theta,in} = 670$, which is consistent with the very similar recoveries of C_f for the two Reynolds numbers observed in figure 3(*a*).

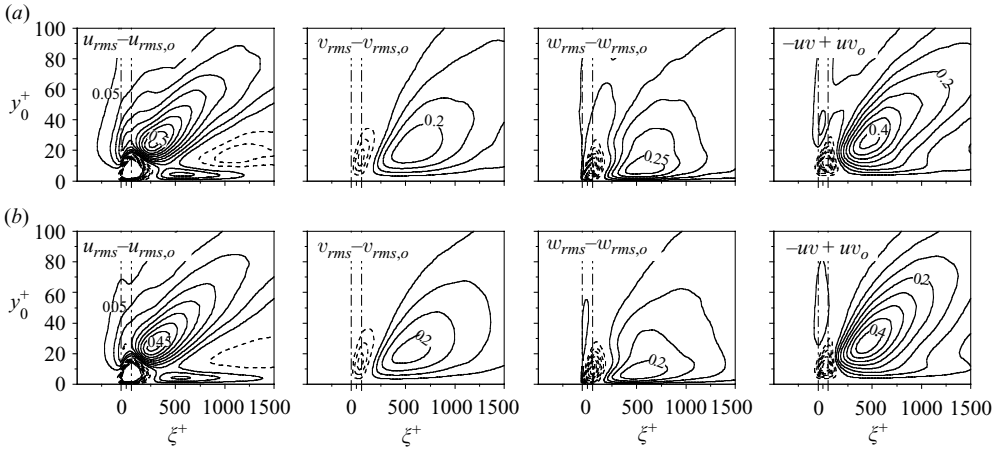

FIGURE 5. Contours of the difference between the time-averaged turbulent intensities and Reynolds shear stress for steady blowing and those for no blowing. Here, $y_o^+ = yu_{\tau,o}/\nu$ and $u_{\tau,o}$ is the local wall-shear velocity for unperturbed flow. The increment of contours is 0.05 normalized by $u_{\tau,o}$. Negative contours are dashed and zero contours are not drawn. (*a*) $Re_\theta = 300$; (*b*) 670.

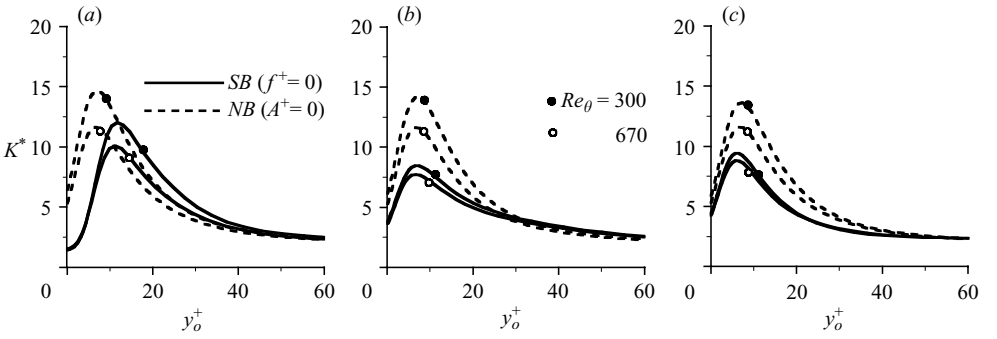

FIGURE 6. Energy partition parameter $K^* = 2\overline{u'^2}/(\overline{v'^2} + \overline{w'^2})$. (*a*) $\xi^+ = 0$; (*b*) 500; (*c*) 1000.

Figure 5 shows contour plots of the differences between the r.m.s. velocity fluctuations (u'_{rms}, v'_{rms}, w'_{rms} and $-\overline{u'v'}$) for the systems with and without blowing. Imposition of the local forcing leads to a decrease in the velocity fluctuations and Reynolds shear stress near the slot because the fluctuating fluid is lifted away from the wall by the blowing. However, the blowing causes a significant increase in the velocity fluctuations and Reynolds shear stress downstream of the slot. For $Re_{\theta,in} = 300$ (figure 5*a*), the global features of v'_{rms}, w'_{rms} and $-\overline{u'v'}$ are similar, but u'_{rms} shows different behaviour. The maximum increase of u'_{rms} is located closer to the slot than those of v'_{rms}, w'_{rms} and $-\overline{u'v'}$. The response of the turbulent intensities observed for $Re_{\theta,in} = 670$ (figure 5*b*) is similar to that for $Re_{\theta,in} = 300$. This provides further evidence that σ^+ is an appropriate quantity for parameterizing the local blowing.

To see the relative contributions to the turbulent kinetic energy of the streamwise turbulent intensity and the intensities normal to the mean flow, the energy partition parameter, $K^* = 2\overline{u'^2}/(\overline{v'^2} + \overline{w'^2})$, was calculated. Above the slot ($\xi^+ = 0$; figure 6*a*), the peak location of K^* is shifted away from the wall because of the blowing. In the downstream, K^* significantly decreases near the wall for both $Re_{\theta,in} = 300$ and

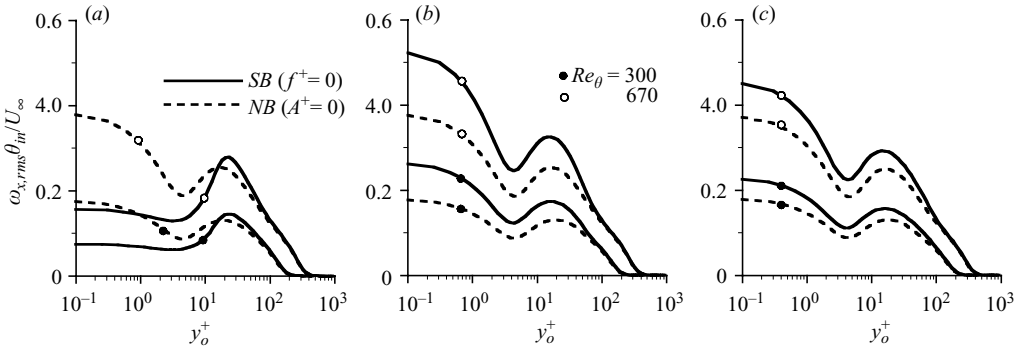

FIGURE 7. Variations of the streamwise vorticity fluctuations due to local blowing. (*a*) $\xi^+ = 0$; (*b*) 500; (*c*) 1000.

670 in comparison with the no-blowing case. The smaller value of K^* indicates that the energy redistribution is more active. Senda *et al.* (1981) showed by examining the integral length scale that turbulence tends to be close to isotropy with injection. Chung, Sung & Krogstad (2002) found that surface blowing activates the transverse components of velocity fluctuations and decreases the anisotropy of the near-wall turbulence significantly. Sumitani & Kasagi (1995) reported that surface blowing enhances the redistribution mechanism of the pressure–strain terms. In figure 6, it is found that the localized blowing applied in the present work also enhances the cross-stream components of the turbulent intensity more than the streamwise component.

Figure 7 shows the variations of the streamwise vorticity fluctuations (ω_x') due to the local blowing. The location of the local maximum in ω_x' corresponds to the average location of the centre of the streamwise vortices (Kim, Moin & Moser 1987). When blowing is applied, the local maximum of ω_x' moves away from the wall above the slot (figure 7*a*), indicating that the quasi-streamwise vortices are lifted up by the blowing. As a result, the magnitude of ω_x' increases in the downstream. Similar behaviour was observed by Park & Choi (1999) in DNSs of steady blowing in a turbulent boundary layer with $Re_{\theta,in} = 300$; they explained their observations in terms of a strengthening of the lifted vortices in the downstream owing to less viscous diffusion (above the slot) and more tilting and stretching (downstream of the slot). Furthermore, Kim, Kim & Sung (2003*b*) reported that the activated streamwise vortices and the relevant motions in the viscous sublayer are responsible for the increase in wall pressure fluctuations, which are detected in figure 3(*c*). Jeong *et al.* (1997) proposed an energy transfer scenario to account for the behaviour of the streamwise vortices, whereby the pressure–strain rate terms in v'^2 and w'^2 budgets are closely related to the vortical motion around the streamwise vortices. This is consistent with our observation that local blowing enhances both the streamwise vortices and the energy redistribution (figure 6). The previous DNS studies on localized blowing showed that streamwise vortices are consistently enhanced by localized blowing with different blowing conditions: several blowing rates (σ) with the same spanwise slot width (Park & Choi 1999); and different blowing magnitudes at a fixed blowing rate (Kim *et al.* 2002*b*). Considering that the near-wall streamwise vortices play a dominant role in wall-bounded flows (Robinson 1991), the activation of streamwise vortices can be regarded as one of the most important effects of localized blowing on a turbulent boundary layer.

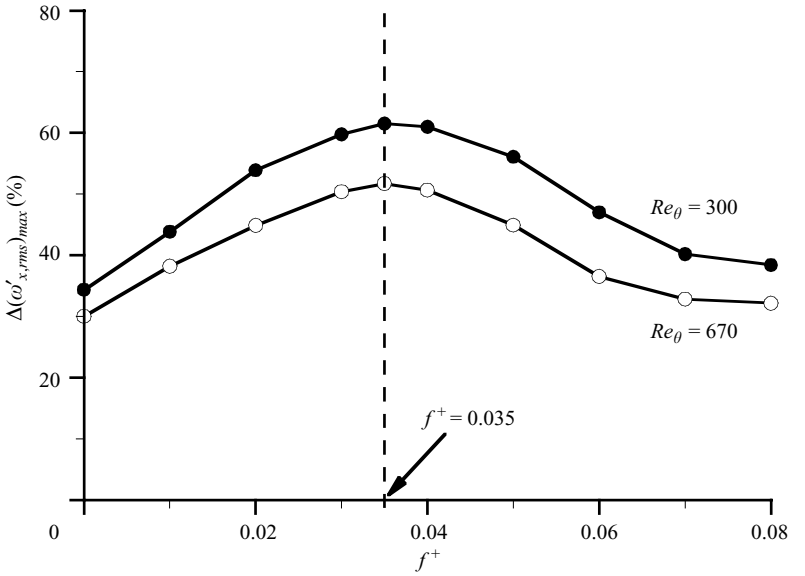

FIGURE 8. Relative increases of local maximum of $\omega'_{x,rms}$ due to local blowing.

4. Localized time-periodic blowing

To investigate the effects of periodic blowing on near-wall turbulence, it is important to elucidate the effect of this type of blowing on the streamwise vorticity fluctuations. The relative increase in the local maximum of streamwise vorticity fluctuations is defined as $\Delta\omega'_{x,max} = (\omega'_{x,max} - \omega'_{x,max,o})/\omega'_{x,max,o} \times 100$, where the subscript '$o$' denotes 'no blowing'. Figure 8 shows the relative increase in $\omega'_{x,max}$ versus the blowing frequency. Here, $f^+ = 0$ corresponds to steady blowing. For both $Re_{\theta,in} = 300$ and 670, $\omega'_{x,max}$ is significantly increased by the periodic blowing up to a maximum at $f^+ = 0.035$. For $Re_{\theta,in} = 300$, $\omega'_{x,max}$ is increased by up to 60 % for periodic blowing, compared to 35 % increase induced by steady blowing. These results suggest that periodic blowing enhances the near-wall streamwise vortices to a greater degree than steady blowing, and that there exists an optimal blowing frequency ($f^+ = 0.035$ in the present study) for the activation of streamwise vortices by localized blowing.

Figure 9 shows the variations of the local maximum values of the streamwise vorticity fluctuations in the streamwise direction. The local maximum of ω'_x is significantly higher in the downstream for the system with local blowing compared with the no-blowing system. The response of $\omega'_{x,max}$ to local blowing is nearly the same as that of the local maximum of the Reynolds shear stress (figure 3). The effect of blowing frequency on the evolution of $\omega'_{x,max}$ is clearly seen in the downstream direction. In the frequency domain where f^+ is lower than the effective frequency ($f^+ < 0.035$), $\omega'_{x,max}$ in the downstream becomes larger for both $Re_{\theta,in} = 300$ and 670 as f^+ increases (figure 9*a*, *c*). For $f^+ > 0.035$, however, $\omega'_{x,max}$ decreases with increasing f^+ and converges to that of the steady blowing system (figure 9*b*, *d*). The effect of periodic blowing on $\omega'_{x,max}$ is confined to the streamwise region of $0 < \xi^+ < 1000$. It is clear that $\omega'_{x,max}$ is most increased at a blowing frequency of $f^+ = 0.035$ for both $Re_{\theta,in} = 300$ and 670, as shown in figure 8. The maximum increase in $\omega'_{x,max}$ is observed at $\xi^+ \approx 300$.

Figure 10 shows the variation of time-averaged skin friction along the streamwise direction owing to periodic blowing. Three blowing frequencies are examined, the

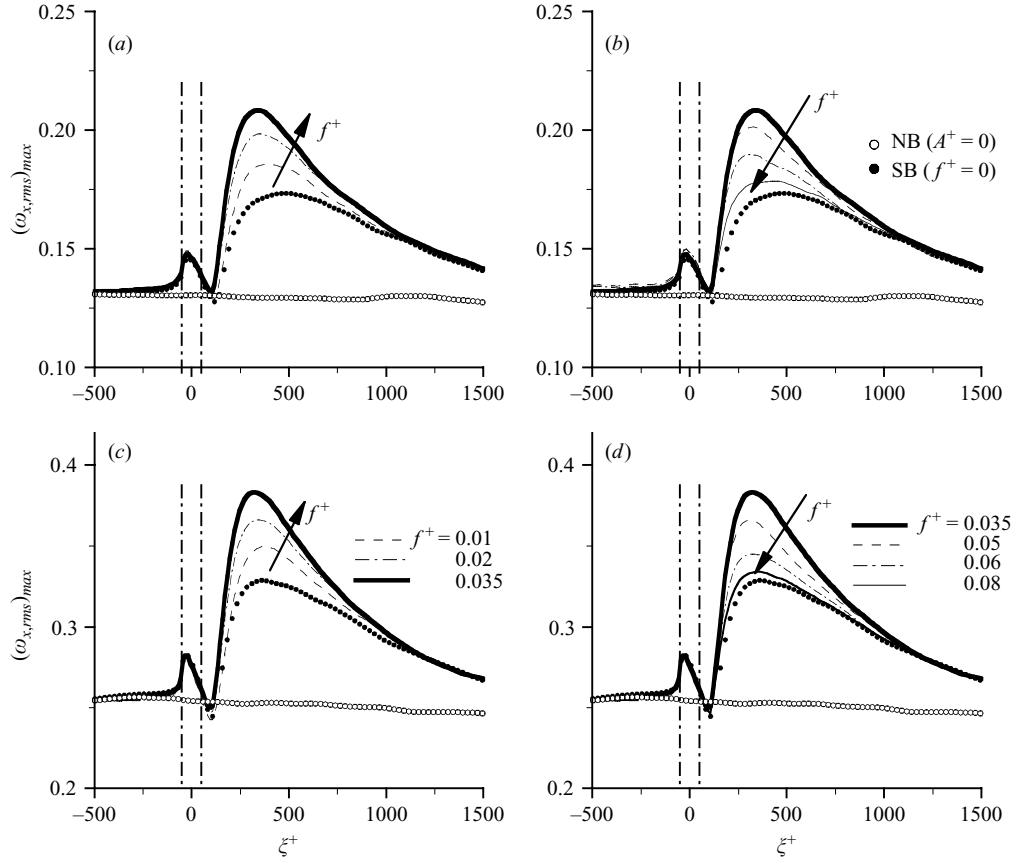

FIGURE 9. Variations of local maximum of $\sqrt{\overline{\omega_x'^2}}\theta_{in}/U_\infty$ in the streamwise direction due to periodic blowing. (a, b) $Re_\theta = 300$; (c, d) 670. (a, c) $f^+ = 0.01$–0.035; (b, d) 0.035–0.08.

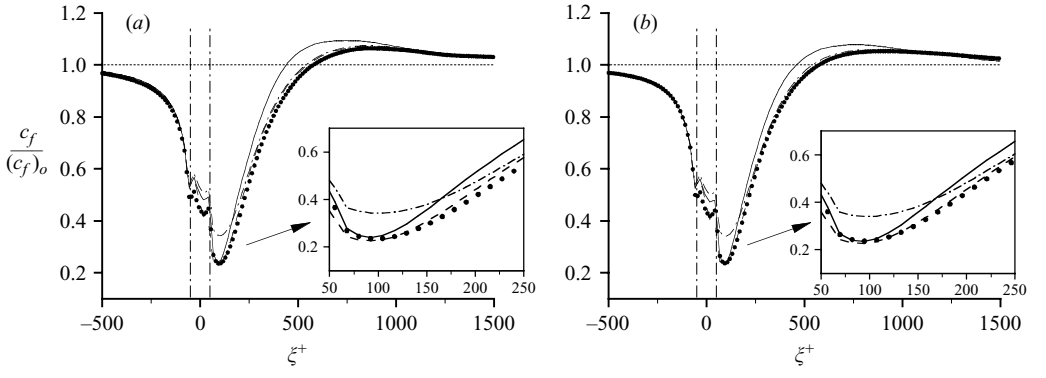

FIGURE 10. Variation of time-averaged skin friction in the streamwise direction due to periodic blowing: –·–, $f^+ = 0.010$; —, $f^+ = 0.035$; - - -, $f^+ = 0.080$; ●, SB ($f^+ = 0$). (a) $Re_\theta = 300$; (b) 670.

effective blowing frequency $f^+ = 0.035$, as well as $f^+ = 0.01$ and 0.08. Blowing at frequency $f^+ = 0.035$ gives the maximum increase in the streamwise vorticity fluctuations. Similarly to steady blowing, C_f for periodic blowing decreases rapidly

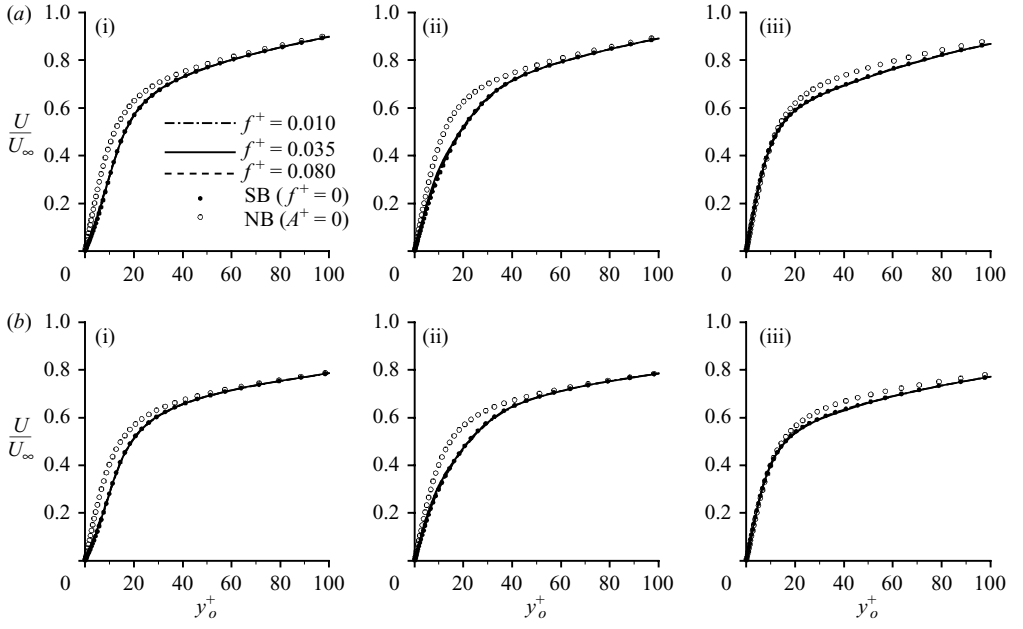

FIGURE 11. Time-averaged streamwise velocity profiles. (*a*) $Re_\theta = 300$; (*b*) 670. (i) $\xi^+ = 0$; (ii) 300; (iii) 900.

near the slot and increases in the downstream. For both $Re_{\theta,in} = 300$ and 670, the skin friction for $f^+ = 0.035$ increases to a higher value in the downstream than other cases. Furthermore, the increasing rate of C_f is largest at $f^+ = 0.035$. Note that the maximum increase of C_f occurs at the effective blowing frequency ($f^+ = 0.035$) for enhancement of $\omega'_{x,max}$. This suggests that in the presence of localized blowing, the increase of skin friction far downstream is closely related to the enhancement of the near-wall streamwise vortices. Close inspection of C_f recovery near the slot indicates that the skin friction of $f^+ = 0.01$ is larger than that of the steady blowing for both Reynolds numbers. Kim & Sung (2003) reported by examining the time-averaged x momentum equation at the wall, that the C_f reduction by periodic blowing is smaller than that by steady blowing. The present results further show that the reduction of skin friction increases with increasing f^+ and converges to that of steady blowing.

The distributions of the time-averaged streamwise velocity at three locations ($\xi^+ = 0$, 300 and 900) are shown in figure 11. Compared to the no-blowing system, a region of retarded flow is observed near the wall ($\xi^+ = 0$). As the flow moves downstream, this region of retarded flow gradually shifts away from the wall and finally decays. However, the time-averaged streamwise velocity is insensitive to the blowing frequency.

Figure 12 shows the velocity profiles of the r.m.s. of the oscillating component for $Re_{\theta,in} = 670$, which are defined as

$$\tilde{u}_{rms} = \sqrt{\overline{(\tilde{u})^2}} = \sqrt{\overline{(\langle u \rangle - \bar{u})^2}},$$

$$\tilde{v}_{rms} = \sqrt{\overline{(\tilde{v})^2}} = \sqrt{\overline{(\langle v \rangle - \bar{v})^2}}.$$

This quantity shows a clear dependence on blowing frequency, in contrast to the insensitivity of the mean velocity to unsteady blowing. As the blowing frequency

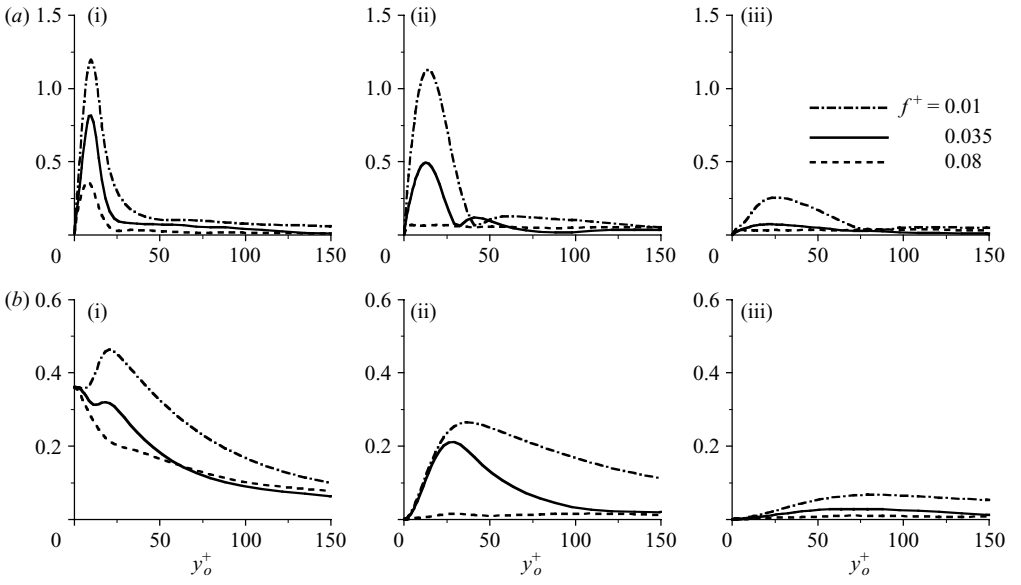

FIGURE 12. Root mean square of oscillating component of phase-averaged velocity ($Re_{\theta,in} = 670$). (*a*) $\tilde{u}_{rms}/u_{\tau,o}$; (*b*) $\tilde{v}_{rms}/u_{\tau,o}$. (i) $\xi^+ = 0$; (ii) 300; (iii) 900.

increases, $\tilde{u}_{rms}$ and $\tilde{v}_{rms}$ decrease. At $\xi^+ = 300$, $\tilde{u}_{rms}$ exhibits a double peak whereas $\tilde{v}_{rms}$ has a single peak. Examination of the phase of $\tilde{u}$ revealed that the double peaks of $\tilde{u}_{rms}$ have a π phase difference, indicating that $\tilde{u}$ has opposite signs above and below the location of the local minimum in $\tilde{u}_{rms}$. Closer inspection of $\tilde{u}_{rms}$ at $\xi^+ = 300$ reveals that, for $f^+ = 0.035$, the second peak is more distinct than is the case for other frequencies. It is also observed that the y location of the minimum in $\tilde{u}_{rms}$ for $f^+ = 0.035$ is closer to the wall than in the $f^+ = 0.01$ system. Similar behaviour is observed for the $Re_{\theta,in} = 300$ system. The behaviour of $\tilde{u}$ and $\tilde{v}$ is consistent with that of the spanwise vortical motion (figure 13); that is, $\tilde{u}$ undergoes the most intensive change, with opposite signs just above and below the centre of the spanwise vortical motion. However, the maximum values of $\tilde{v}$ are located just upstream and downstream of the vortical motion at the same y location. The centre of the spanwise vortical motion coincides with the maximum $\tilde{v}_{rms}$, which further shows a close agreement with the location of the local minimum of $\tilde{u}_{rms}$ (Park *et al.* 2001).

Figure 13 shows contour plots of the difference between the phase-averaged spanwise vorticity for periodic blowing $\langle\omega_z\rangle$ and the time-averaged spanwise vorticity for the system without blowing, $\bar{\omega}_{z,o}$, during one period ($1T$) in the $Re_{\theta,in} = 670$ system. For all three blowing frequencies considered ($f^+ = 0.01$, 0.035 and 0.08), a region of negative $\Delta\langle\omega_z\rangle$ appears above the slot because the blowing causes a negative spanwise vorticity layer in the vicinity of the wall to be shifted upward. Note that the negative (positive) value of $\Delta\langle\omega_z\rangle$ represents an increase (decrease) of the magnitude of the spanwise vorticity because $\bar{\omega}_{z,o}$ is negative inside the boundary layer. For $f^+ = 0.01$, a region of strong negative vorticity is formed above the slot and convects downstream with time. During the accelerating phase ($t = 0/4T \sim 1/4T$), a region of strong negative vorticity forms above the slot owing to the blowing-induced lifting of the wall vorticity layer. This region of strong negative spanwise vorticity convects downstream during the decelerating phase ($t = 2/4T \sim 3/4T$), during which the adverse pressure gradient decreases above the slot. For $f^+ = 0.035$, a newly

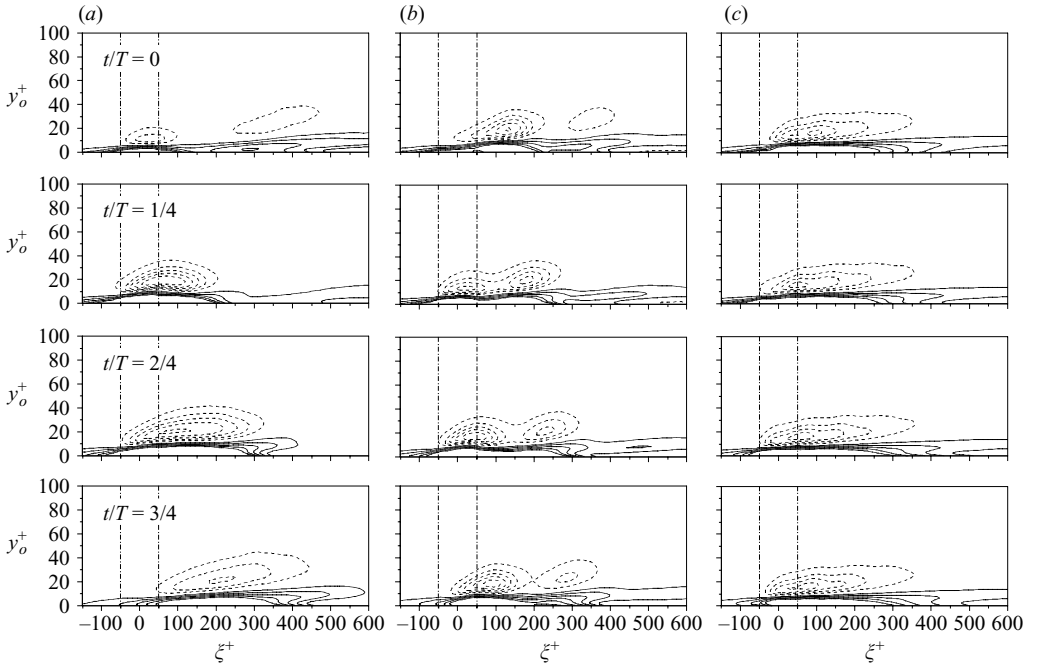

FIGURE 13. Contours of phase-averaged spanwise vorticity $(\langle\omega_z\rangle - \overline{\omega}_{z,o})\theta_{in}/U_\infty$ for $Re_{\theta,in} = 670$. The contour levels are from −0.5 to 0.5 by increments of 0.1. The dashed lines denote the negative value. (*a*) $f^+ = 0.01$; (*b*) 0.035; (*c*) 0.08.

generated region of strong spanwise vorticity coexists with the weaker prior one which convected in the decelerating phase of the previous period. The negative $\Delta\langle\omega_z\rangle$ region has a streamwise wavelength $\lambda_x^+ = 200$. The convection velocity of the region of $\Delta\langle\omega_z\rangle < 0$ is $7.28u_{\tau,o}$ in figure 13(*b*), which is close to the relation of the phase velocity $V_c^+ = f^+\lambda^+ = 7$. For $f^+ = 0.08$, however, the phase difference is so small that the aforementioned responses, such as the convection of the negative $\Delta\langle\omega_z\rangle$, are not observed.

Figure 14 shows the profiles of the time-averaged turbulent intensities and Reynolds shear stress for $Re_{\theta,in} = 670$ at $\xi^+ = 300$, the location where the maximum increase in $\omega'_{x,max}$ occurs. The velocity fluctuations and Reynolds shear stress are increased by application of blowing. The increase in u'_{rms} for $f^+ = 0.035$ is smaller than those for other frequencies, whereas the increases in v'_{rms}, w'_{rms} and $-\overline{u'v'}$ for $f^+ = 0.035$ are larger than those for other frequencies. This suggests that $f^+ = 0.035$ is the most effective blowing frequency in terms of promoting energy transfer between the components of the velocity fluctuations. The same conclusion is drawn for $Re_{\theta,in} = 300$.

Power spectra of the velocity fluctuations, E_{uu}, E_{vv} and E_{ww} at $\xi^+ = 300$ for $Re_{\theta,in} = 670$ are shown in figure 15. To examine the effect of periodic blowing ($f^+ = 0.035$), the spectra for steady blowing and no blowing are plotted together. The spectra show that the flow is reasonably well resolved. As seen in figure 15(*a*), the spectra of E_{uu} are increased by both periodic and steady blowing. E_{uu} of $f^+ = 0.035$ is nearly the same as that of steady blowing at high wavenumber. Around $k_z\theta_{in} = 1.5$, however, E_{uu} of $f^+ = 0.035$ is slightly smaller than that of steady blowing. This is consistent with the smaller increase of u'_{rms} by $f^+ = 0.035$ than that by steady blowing (figure 14*a*). For the cross-stream components, both E_{vv} and E_{ww} are increased in the

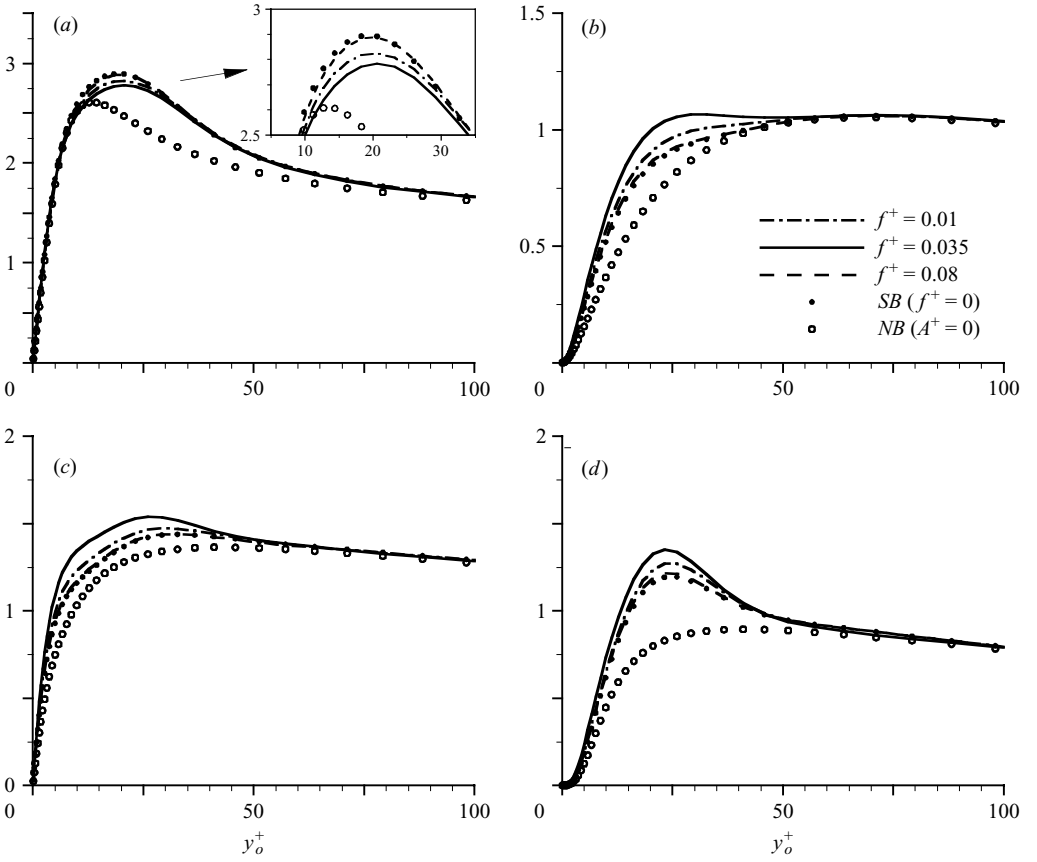

FIGURE 14. Time-averaged turbulent intensities and Reynolds shear stress at $\xi^+ = 300$ for $Re_{\theta,in} = 670$. (*a*) $u'_{rms}/u_{\tau,o}$; (*b*) $v'_{rms}/u_{\tau,o}$; (*c*) $w'_{rms}/u_{\tau,o}$; (*d*) $-\overline{u'v'}/u_{\tau,o}^2$.

low wavenumber, as well as high wavenumber, by the blowings (figures 15*b*, *c*). The increase of energy in the low wavenumber by $f^+ = 0.035$ is larger than that by steady blowing. E_{vv} is significantly changed by the periodic blowing in the low wavenumber. For no blowing, E_{vv} has a dominant peak at $k_z\theta_{in} = 2.0$, which corresponds to the wavelength $\lambda_z^+ = 103$. However, for $f^+ = 0.035$, the spectrum E_{vv} is much increased at low wavenumber ($k_z\theta_{in} < 1.0$) where the peak is not clearly detected.

The transport equations for Reynolds stress can provide additional information on the effect of periodic blowing on the near-wall turbulence transport. The transport equation for the phase-averaged Reynolds stress components can be written as

$$0 = \underbrace{-\frac{\partial\langle u_i'u_j'\rangle}{\partial t} - \langle u_k\rangle\frac{\partial\langle u_i'u_j'\rangle}{\partial x_k}}_{C_{ij}} \underbrace{-\left(\langle u_i'u_k'\rangle\frac{\partial\langle u_j\rangle}{\partial x_k} + \langle u_i'u_k'\rangle\frac{\partial\langle u_j\rangle}{\partial x_k}\right)}_{P_{ij}}$$
$$\underbrace{-\frac{\partial\langle u_i'u_j'u_k'\rangle}{\partial x_k}}_{T_{ij}} \underbrace{-\frac{2}{Re}\left\langle\frac{\partial u_i'}{\partial x_k}\frac{\partial u_j'}{\partial x_k}\right\rangle}_{\varepsilon_{ij}} + \underbrace{\frac{1}{Re}\frac{\partial^2\langle u_i'u_j'\rangle}{\partial x_k^2}}_{D_{ij}} \underbrace{-\left\langle u_i'\frac{\partial p'}{\partial x_j} + u_j'\frac{\partial p'}{\partial x_i}\right\rangle}_{\Pi_{ij}}. \qquad (21)$$

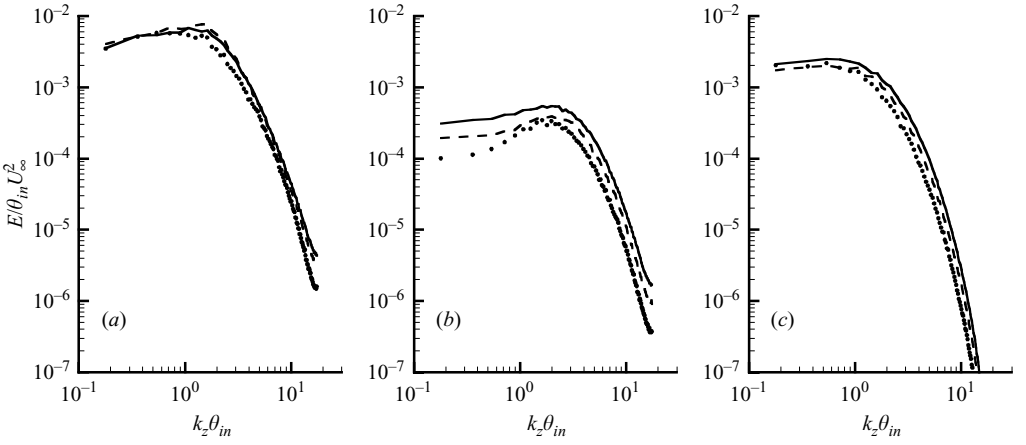

FIGURE 15. One-dimensional energy spectra at $(\xi^+, y_o^+) = (300, 21)$ for $Re_{\theta,in} = 670$: —, $f^+ = 0.035$; - - -, SB ($f^+ = 0$); ●, NB ($A^+ = 0$). (*a*) E_{uu}; (*b*) E_{vv}; (*c*) E_{ww}.

The terms on the right-hand side of (21) represent: C_{ij} = convection, P_{ij} = production, T_{ij} = turbulent transport, ε_{ij} = dissipation, D_{ij} = viscous diffusion and Π_{ij} = velocity pressure-gradient. Note that C_{ij} represents the rate of change of the Reynolds stress following a point moving with the local phase-averaged velocity $\langle \boldsymbol{u} \rangle$. To investigate the greater increase of the cross-stream components of the turbulent intensity compared to the streamwise component at $f^+ = 0.035$, we calculated the budget terms for the Reynolds normal stresses in (21). Figure 16 shows the budget terms in the phase-averaged Reynolds stress transport equation at $\xi^+ = 300$ for $f^+ = 0.035$ ($Re_{\theta,in} = 670$). The budgets normalized by $u_{\tau,o}^4/\nu$ are displayed during one period ($1T$). The $\langle u'^2 \rangle$ budgets (figure 16*a*) show that the production term is dominant, similar to the behaviour of the unperturbed turbulent boundary-layer flow (Spalart 1988). The velocity pressure-gradient term becomes significant near $y_o^+ = 25$, where the magnitude of Π_{11} is even larger than that of dissipation at $t/T = 2/4$. The budgets of the wall-normal stress component $\langle v'^2 \rangle$ are shown in figure 16(*b*). In the absence of blowing, the dissipation term ε_{22} is the dominant consuming term and the velocity pressure-gradient term Π_{22} is the dominant producing term (Na & Moin 1996). The increase in Π_{22} is most significant at $f^+ = 0.035$ compared to other blowing frequencies (not shown here). The production term, which is negligible through the layer without forcing, becomes dominant at the phase of $t/T = 2/4$. This increase in P_{22} is closely related to the spanwise vortical motion of the phase-averaged velocity field (Kim & Sung 2003). As seen in figure 13(*b*), the negative spanwise vortical structure induces a 'downwash' at $\xi^+ = 300$ in $t/T = 2/4$, which gives $\partial\langle v \rangle/\partial y < 0$ at the right-hand bottom of the vortical structure. The oscillating components of the strain rate enhance the production term $P_{22} = -2(\langle v'^2 \rangle(\partial\langle v \rangle/\partial y) + \langle u'v' \rangle(\partial\langle v \rangle/\partial x))$. However, the time-averaged production term $\overline{P_{22}}$ in the $\overline{v'^2}$ budgets is negligible compared with the velocity pressure-gradient term. In the budget of $\langle w'^2 \rangle$ (figure 16*c*), the velocity pressure-gradient term is dominant and is balanced by the dissipation term except very near the wall where the viscous diffusion is very important; this behaviour is similar to that of the no-blowing system. Similar to Π_{22}, the increase in Π_{33} is greater at $f^+ = 0.035$ than at other blowing frequencies (not shown here).

To see the contribution of the oscillating strain rate due to periodic blowing to the production term of the Reynolds stress, the time-averaged production term

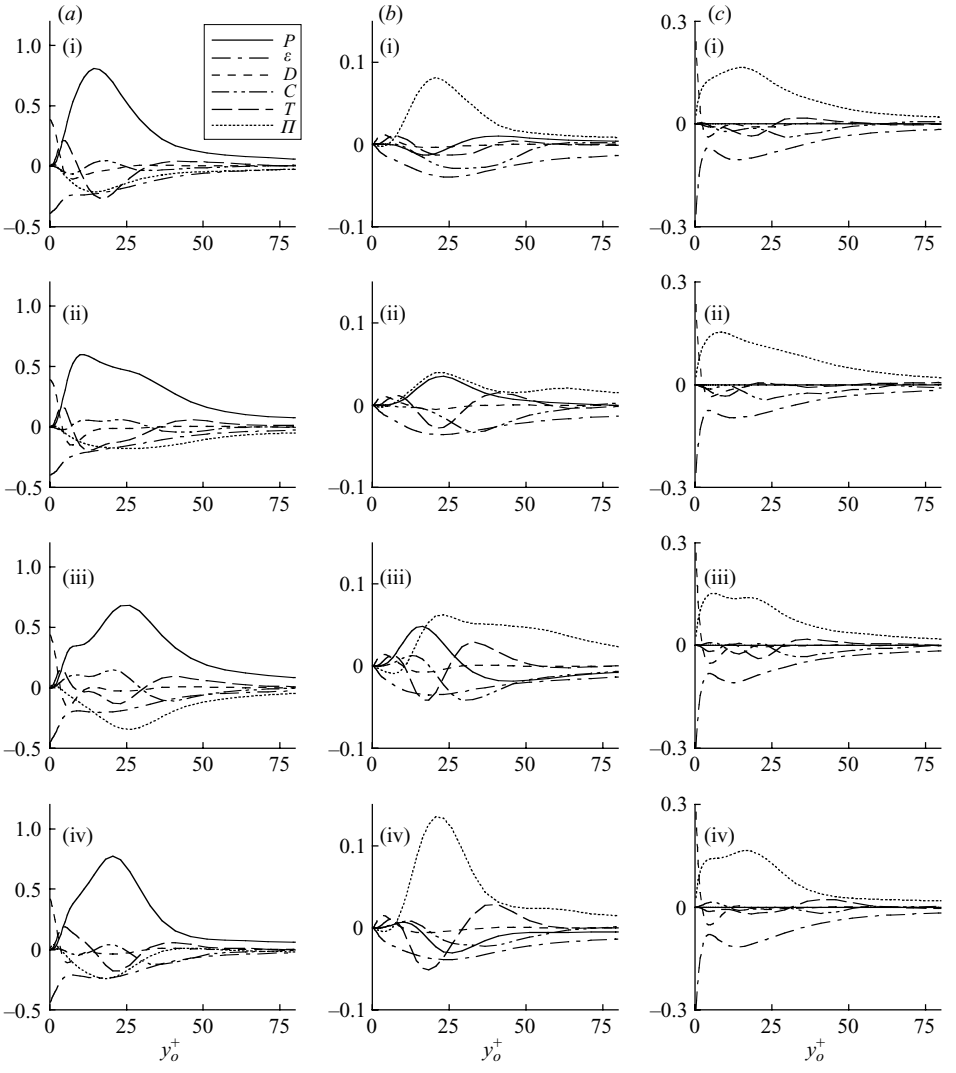

FIGURE 16. Variations of terms in the phase-averaged Reynolds stress transport equation at $\xi^+ = 300$ for $f^+ = 0.035$ ($Re_{\theta,in} = 670$). The budgets are normalized by $u_{\tau,o}^4/\nu$. (*a*) $\langle u'^2 \rangle$ budgets; (*b*) $\langle v'^2 \rangle$ budgets; (*c*) $\langle w'^2 \rangle$ budgets. (i) $t/T = 0/4$; (ii) 1/4; (iii) 2/4; (iv) 3/4.

for $f^+ = 0.035$ is examined. The time-averaged production term for the periodic blowing can be expressed as

$$\overline{P_{ij}} = -\left(\overline{u_i' u_k'} \frac{\partial \bar{u}_j}{\partial x_k} + \overline{u_j' u_k'} \frac{\partial \bar{u}_i}{\partial x_k}\right) - \left[\overline{\widetilde{u_i' u_k'} \frac{\partial \tilde{u}_j}{\partial x_k}} + \overline{\widetilde{u_j' u_k'} \frac{\partial \tilde{u}_i}{\partial x_k}}\right]. \tag{22}$$

Here, the second group in brackets represents the interaction between the oscillating components due to periodic blowing. Figure 17 shows the time-averaged production terms $\overline{P_{11}}$, $\overline{P_{22}}$ and $\overline{P_{12}}$ for the $Re_{\theta,in} = 670$ system subjected to blowing at frequency $f^+ = 0.035$. The interaction between the oscillating components is much smaller than the first bracketed group in (22). The terms in (22) giving the greatest contributions to

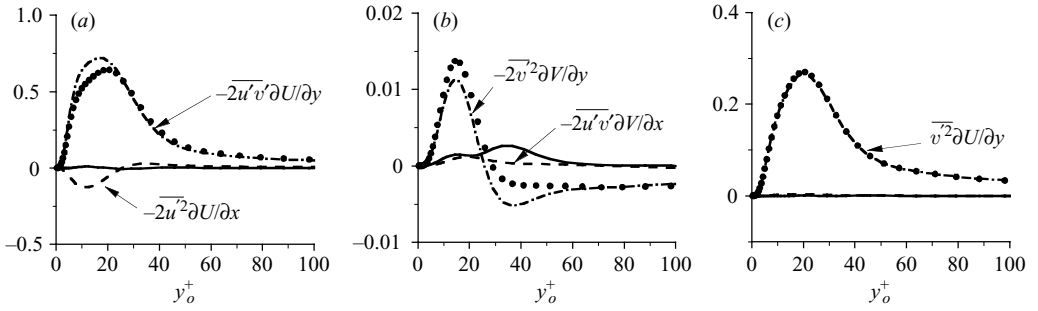

FIGURE 17. Time-averaged production terms normalized by $u_{\tau,o}^4/\nu$ at $\xi^+ = 300$ for $f^+ = 0.035$ ($Re_{\theta,in} = 670$). (*a*) $\bar{P}_{11}$; (*b*) $\bar{P}_{22}$; (*c*) $\bar{P}_{12}$. ●, total production; —, interaction between oscillating terms.

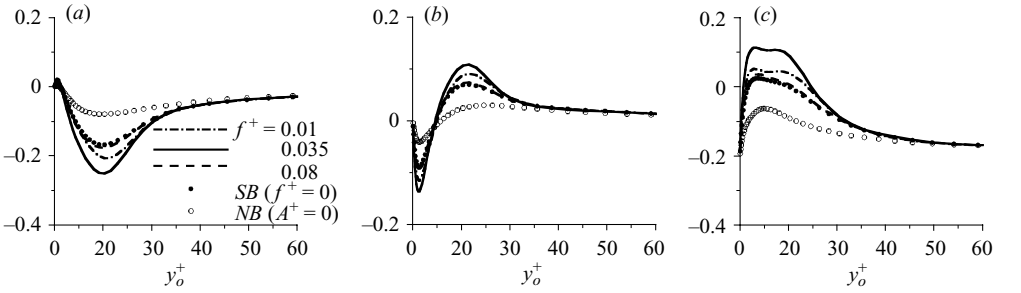

FIGURE 18. Pressure–strain correlation terms at $\xi^+ = 300$ for $Re_{\theta,in} = 670$. (*a*) $\phi_{11}\nu/u_{\tau,o}^4$; (*b*) $\phi_{22}\nu/u_{\tau,o}^4$; (*c*) $\phi_{33}\nu/u_{\tau,o}^4$.

$\overline{P_{11}}$, $\overline{P_{22}}$ and $\overline{P_{12}}$ are $-2\overline{u'v'}\partial U/\partial y$, $-2\overline{v'^2}\partial V/\partial y$ and $\overline{v'^2}\partial U/\partial y$, respectively. Note that these dominant terms contain the wall-normal gradient of the mean velocity. Tardu (1998) reported that the interactions between oscillating components in the production term are non-negligible, since the time mean flow characteristics in his experiments were affected by the imposed unsteadiness. However, our DNS results show that the contribution of the interaction to the time-averaged production is negligible, although the time-averaged production terms for periodic blowing ($f^+ = 0.035$) are larger than those for steady blowing. Considering the insensitivity of the time-mean velocity to the imposed unsteadiness (figure 11), these larger values of $\overline{P_{ij}}$ in the present periodic blowing systems may be attributed to the fact that the periodic blowing enhances $\overline{v'^2}$ and $-\overline{u'v'}$ more than the steady blowing does (figure 14). For more details on the turbulence statistics budgets, see Kim (2005).

To investigate the inter-component energy transfer among the Reynolds-stress components, the time-averaged pressure–strain correlation terms $\phi_{ij} = \overline{p'(\partial u_i'/\partial x_j + \partial u_j'/\partial x_i)}$ near the wall were examined (figure 18). It is known that the pressure–strain term ϕ_{ij} plays a dominant role in the energy redistribution among the components. In the turbulent kinetic energy budget, there is no net contribution from the pressure–strain term. Therefore, a negative sign of ϕ_{kk} (no summation on k) indicates a loss of energy from $u_k'^2$ or a transfer of energy from this component to other components, whereas a positive sign denotes an energy gain. A previous DNS study of turbulent channel flow with blowing found that ϕ_{ij} was

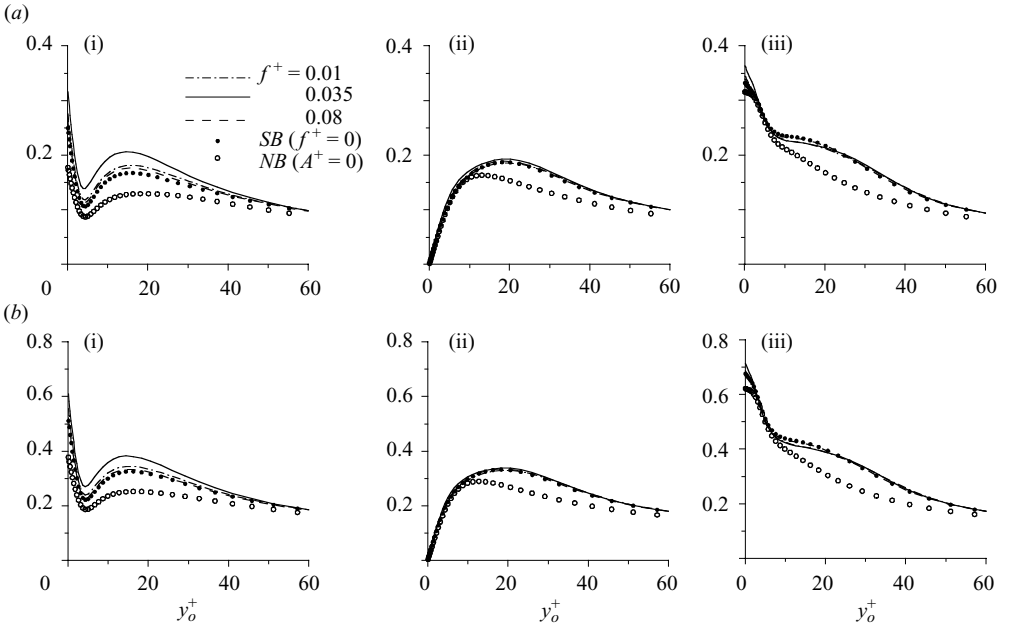

FIGURE 19. Root time–mean square of the vorticity fluctuations at $\xi^+ = 300$. (*a*) $Re_\theta = 300$; (*b*) 670. (i) $\omega'_{x,rms}\theta_{in}/U_\infty$; (ii) $\omega'_{y,rms}\theta_{in}/U_\infty$; (iii) $\omega'_{z,rms}\theta_{in}/U_\infty$.

significantly enhanced in the downstream by local blowing (Chung & Sung 2001). The present results show that ϕ_{ij} is enhanced by periodic blowing and is strongly dependent on the blowing frequency. The magnitude of ϕ_{ij} is increased to the greatest extent by the effective blowing frequency $f^+ = 0.035$. Note that the enhancement of ϕ_{ij} for $f^+ = 0.035$ is nearly twice that achieved using steady blowing, and ϕ_{ij} for $f^+ = 0.08$ is nearly the same as that for steady blowing. This indicates that the energy redistribution is most enhanced at $f^+ = 0.035$, in agreement with the behaviour of the turbulent intensities shown in figure 14.

The intensities of the vorticity fluctuations as a function of y_o^+ are shown in figure 19. All of the components of the vorticity fluctuations (ω'_x, ω'_y and ω'_z) are enhanced by localized blowing. It is clearly seen that ω'_x is enhanced to the greatest extent by the blowing frequency of $f^+ = 0.035$. The location of the local maximum is several wall units closer to the wall in the system with blowing compared to that without. In contrast, varying the blowing frequency has no discernible effect on ω'_y and ω'_z.

To examine the response of the streamwise vorticity fluctuations to periodic blowing, we examined the phase-averaged streamwise vorticity fluctuations during one period ($1T$). A sequence of contour plots of $\langle\omega'_x\rangle^{1/2}$ is shown in figure 20. Vector plots of the oscillating velocity components are superimposed to gain a better understanding of the flow evolution. The response of ω'_x is closely related to the oscillating velocity field. Immediately downstream of the slot, a downward motion is induced at $\xi^+ = 200$ in $t/T = 0/4$, where ω'_x starts to increase and convects downstream. This downward motion enhances the stretching term of the ω'_x transport equation (see below). On the other hand, the blowing also induces an upward motion at $\xi^+ = 300$ in $t/T = 0/4$. This upward motion lifts the strengthened layer of ω'_x formed as a result of the downward motion, thereby weakening the interaction between the strengthened layer of ω'_x and the wall, and causing the lifted vortices to become stronger. For the blowing

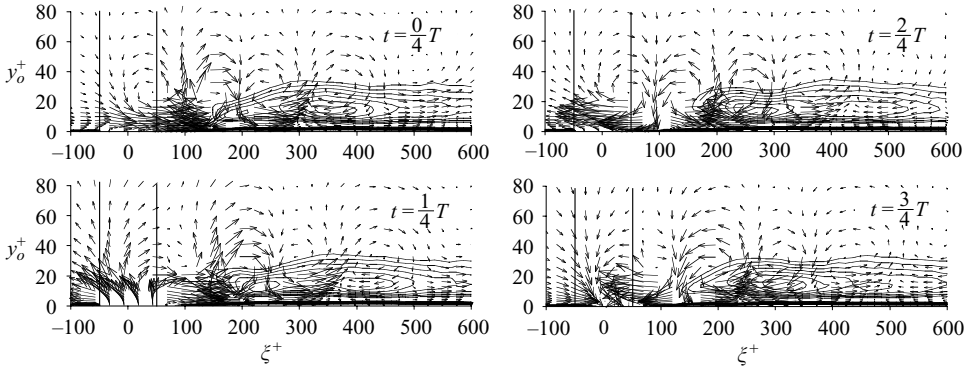

FIGURE 20. Contours of phase-averaged streamwise vorticity $\sqrt{\langle\omega_x'^2\rangle}\theta_{in}/U_\infty$ and vector plots of oscillating velocities for $f^+=0.035$ ($Re_{\theta,in}=670$). The contour levels are from 0.30 to 0.45 by increments of 0.015.

frequency of $f^+=0.035$, the streamwise wavelength of the downward and upward motions is approximately 200 wall units, which matches well with the streamwise length scale of near-wall vortical structures (Jeong *et al.* 1997). This suggests that one streamwise vortex undergoes both the downward and upward motions, and that this phenomenon is responsible for the maximum increase in ω_x' at the optimal blowing frequency ($f^+=0.035$).

To investigate the increase in the streamwise vorticity in the aforementioned upward and downward motion in greater detail, the transport equation of the strength of the streamwise vorticity is examined. The streamwise vorticity equation can be written as

$$\frac{\mathrm{D}\omega_x}{\mathrm{D}t}=\omega_x\frac{\partial u}{\partial x}+\omega_y\frac{\partial u}{\partial y}+\omega_z\frac{\partial u}{\partial z}+\frac{1}{Re}\nabla^2\omega_x, \tag{23}$$

where $\mathrm{D}/\mathrm{D}t=\partial/\partial t+u_j\partial/\partial x_j$. The four terms on the right-hand side represent the enhancement of ω_x due to stretching, the tilting of ω_y, the twisting of ω_z, and viscous diffusion, respectively. Substituting in (23) for ω_y and ω_z yields

$$\frac{\mathrm{D}\omega_x}{\mathrm{D}t}=\omega_x\frac{\partial u}{\partial x}-\frac{\partial w}{\partial x}\frac{\partial u}{\partial y}+\frac{\partial v}{\partial x}\frac{\partial u}{\partial z}+\frac{1}{Re}\nabla^2\omega_x. \tag{24}$$

Multiplying (24) by ω_x gives the dynamic equation for the strength of the streamwise vorticity (Park & Choi 1999),

$$\frac{1}{2}\frac{\mathrm{D}\omega_x^2}{\mathrm{D}t}=\underbrace{\omega_x^2\frac{\partial u}{\partial x}}_{\mathrm{ST}}-\underbrace{\omega_x\frac{\partial w}{\partial x}\frac{\partial u}{\partial y}}_{\mathrm{TT1}}+\underbrace{\omega_x\frac{\partial v}{\partial x}\frac{\partial u}{\partial z}}_{\mathrm{TT2}}+\omega_x\frac{1}{Re}\nabla^2\omega_x. \tag{25}$$

By examining each term on the right-hand side of (25), we can determine which term is dominant in producing the blowing-induced enhancement of the streamwise vorticity. The first three terms on the right-hand side of (25) represent: ST = contribution due to stretching of ω_x, TT1 = net contribution due to the tilting of ω_y, TT2 = net contribution due to the twisting of ω_z on the enhancement of the streamwise vorticity strength. Figure 21(*a*) shows the time-averaged values of the stretching and tilting terms in the absence of blowing. TT2 is negligible compared with the other terms (ST and TT1), consistent with the results of Brooke & Hanratty (1993). For $y_o^+<10$, the tilting term dominates, whereas the stretching term has nearly the same magnitude

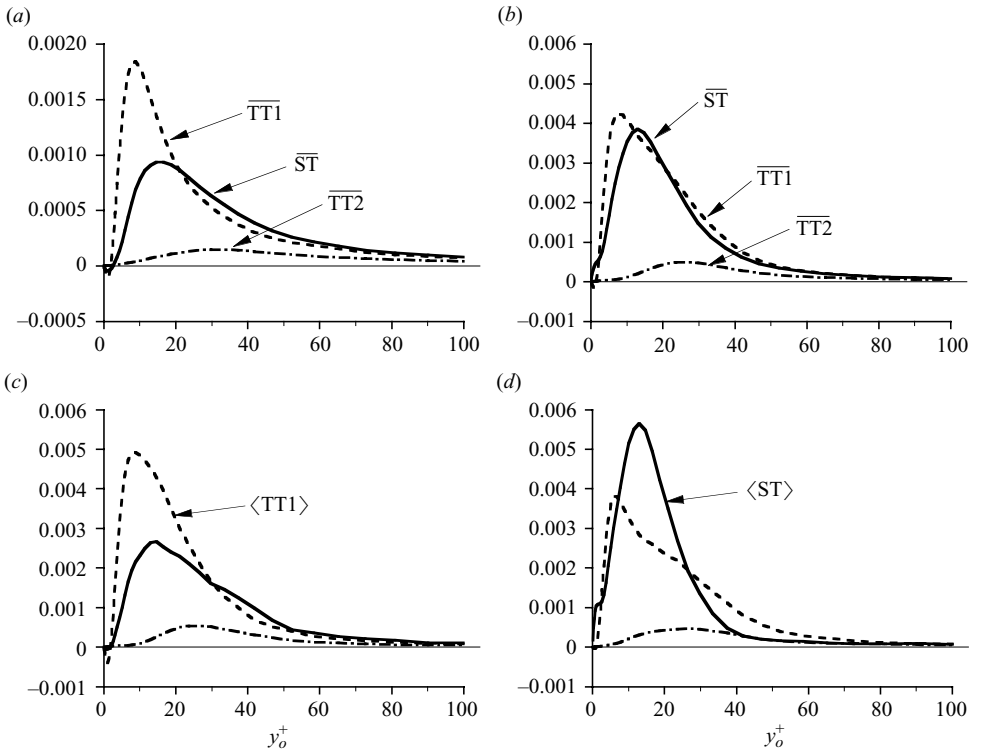

FIGURE 21. Stretching and tilting terms of streamwise vorticity transport equations at the location of $\xi^+ = 300$ for $Re_{\theta,in} = 670$. (*a*) Time-averages for NB, (*b*) Time-averages for $f^+ = 0.035$, (*c*) Phase-averages at $t = 0/4T$ for $f^+ = 0.035$, (*d*) Phase-averages at $t = 2/4T$ for $f^+ = 0.035$.

as the tilting term for $y_o^+ > 20$. The time-averaged values of the stretching and tilting terms at $\xi^+ = 300$ are shown in figure 21(*b*) for the system with periodic blowing at the optimal frequency ($f^+ = 0.035$). Note that the stretching and tilting terms for the periodic blowing are about twice as large as those for the system without blowing (figure 21*a*). The stretching term is significantly enhanced and dominates even near the wall ($y_o^+ < 10$), in contrast to the behaviour of the system without blowing. For the phase at which the upward and downward motions take place at $\xi^+ = 300$, the phase-averaged stretching and tilting terms are represented in figures 21(*c*) and 21(*d*), respectively. At the phase of the upward motion, the stretching and tilting terms are increased compared with the corresponding terms for the no-blowing system; however, the relative contribution of each term is nearly the same as for the system without blowing. At the phase of the downward motion, on the other hand, the stretching term is increased to such an extent that it is larger than the tilting term TT1 at $y_o^+ = 20$. In the downward motion, the streamwise vortices move closer to the wall and a negative $\tilde{v}$ toward the wall indicates that the flow spreads out near the wall, which enhances the stretching term owing to the increased $\partial u/\partial x > 0$ as the flow spreads out.

A quantitative statistical description of the relationship between the streamwise vorticity ω_x' and each term in the ω_x' transport (24), is obtained from the correlation coefficients $R_{\omega_x\omega_x}$, $R_{\omega_x \mathrm{ST}}$ and $R_{\omega_x \mathrm{TT1}}$, which are defined as

$$R_{\omega_x\omega_x}(\Delta x, y, \Delta z) = \frac{\langle \omega_x'(x_{ref}, y_{ref}, z) \times \omega_x'(x_{ref} + \Delta x, y, z + \Delta z) \rangle}{\omega_{x,rms}'(x_{ref}, y_{ref}) \times \omega_{x,rms}'(x_{ref} + \Delta x, y)}, \tag{26}$$

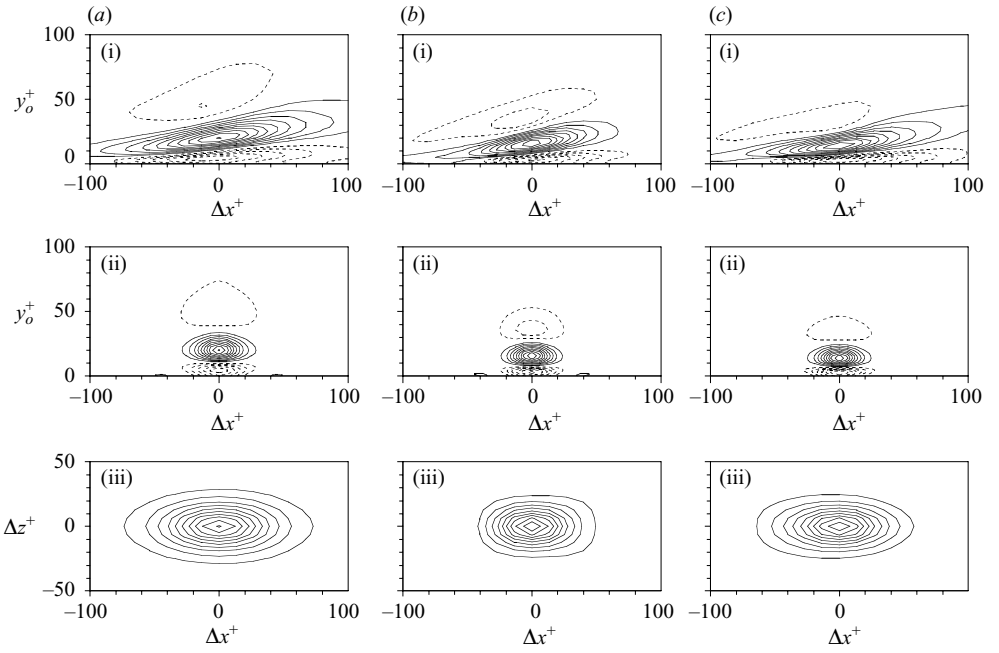

FIGURE 22. Contours of $R_{\omega_x\omega_x}(\Delta x, y, \Delta z)$ for $Re_{\theta,in} = 670$. (*a*)(i)–(iii), No blowing case; (*b*)(i)–(iii), Upward motion phase at $\xi^+ = 300$ for $f^+ = 0.035$ ($t = 0/4T$); (*c*)(i)–(iii), Downward motion phase at $\xi^+ = 300$ for $f^+ = 0.035$ ($t = 2/4T$). (*a*)(i)–(*c*)(i), at $\Delta z^+ = 0$ in the (x, y)-plane; (*a*)(ii)–(*c*)(ii), at $\Delta x^+ = 0$ in the (z, y)-plane; (*a*)(iii)–(*c*)(iii), at $y^+ = y_{ref}$ in the (x, z)-plane. The contour levels are from −1.0 to 1.0 in increments of 0.1. Negative contours are dashed and zero contours are not drawn.

$$R_{\omega_x \mathrm{ST}}(\Delta x, y, \Delta z) = \frac{\left\langle \omega_x'(x_{ref}, y_{ref}, z) \times \left(\omega_x' \frac{\partial u}{\partial x}\right)'(x_{ref} + \Delta x, y, z + \Delta z) \right\rangle}{\omega_{x,rms}'(x_{ref}, y_{ref}) \times \left(\omega_x' \frac{\partial u}{\partial x}\right)'_{rms}(x_{ref} + \Delta x, y)}, \quad (27)$$

and

$$R_{\omega_x \mathrm{TT1}}(\Delta x, y, \Delta z) = \frac{\left\langle \omega_x'(x_{ref}, y_{ref}, z) \times \left(-\frac{\partial w}{\partial x}\frac{\partial u}{\partial y}\right)'(x_{ref} + \Delta x, y, z + \Delta z) \right\rangle}{\omega_{x,rms}'(x_{ref}, y_{ref}) \times \left(-\frac{\partial w}{\partial x}\frac{\partial u}{\partial y}\right)'_{rms}(x_{ref} + \Delta x, y)}, \quad (28)$$

respectively. Using the database of the DNS of a turbulent boundary layer at $Re_{\theta,in} = 670$, the correlation coefficients are obtained and the reference location (x_{ref}, y_{ref}) is $(\xi^+ = 300, y^+_{\omega_x,max})$, where $y^+_{\omega_x,max}$ is the wall normal location of maximum $\omega_{x,rms}'$.

Contours of the two-point autocorrelation coefficient of ω_x' are shown in figure 22. For the phases when the upward and downward motions take place at $\xi^+ = 300$, the correlation coefficients are displayed in figures 22(*b*) and 22(*c*), respectively. For reference, the correlation coefficients for no-blowing are shown in figure 22(*a*). For no blowing, the correlation shows an elongated positive region in the streamwise direction, which corresponds to the well-known streamwise vortical structure. The

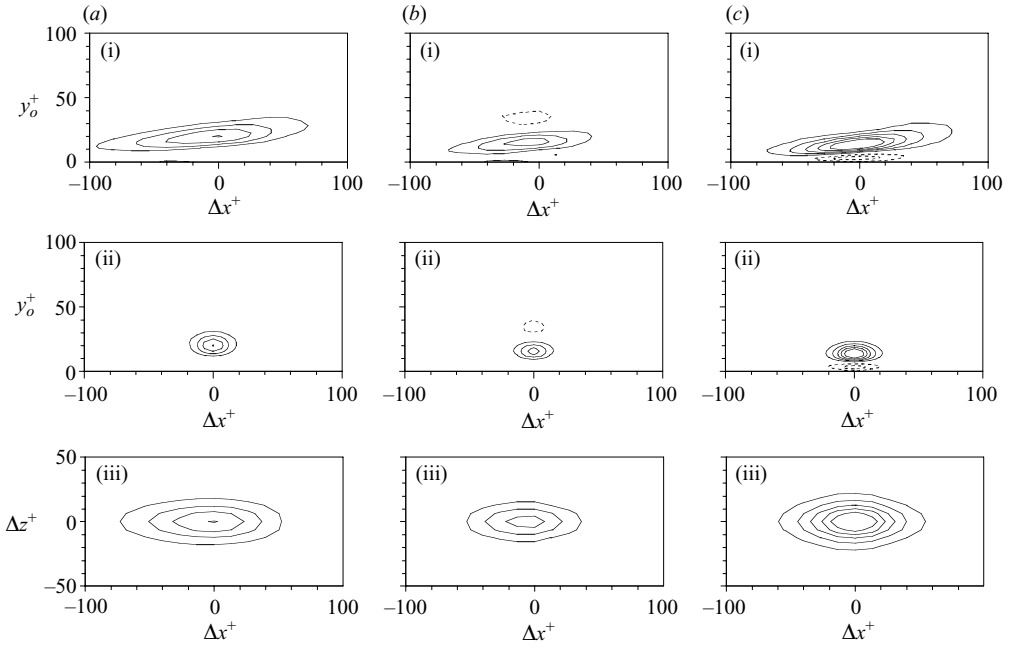

FIGURE 23. Contours of $R_{\omega_x \mathrm{ST}}(\Delta x, y, \Delta z)$ for $Re_{\theta,in} = 670$. (*a*) NB ($A^+ = 0$); (*b*) upward motion; (*c*) downward motion.

streamwise structure with positive correlation has a streamwise extent of 200 wall units and a diameter of 25 wall units. The inclination angle of the structure is about 8.3°, which is close to the value of 9° obtained by Jeong *et al.* (1997) for a turbulent channel flow ($Re_\tau = 180$). The negative correlation near the wall is due to the opposite signed ω_x' induced by the streamwise vortices as a result of the no-slip condition at the wall. The correlation also shows a negative value above the streamwise vortical structure ($y^+ > 30$). This is consistent with the educed streamwise vortical structure observed by Jeong *et al.* (1997), in which the positive-signed and negative-signed streamwise vortices overlap each other in the streamwise direction. In the upward motion (figure 22*b*), the head of the vortical structure is considerably shortened and the streamwise length scale of $R_{\omega_x \omega_x}$ decreases significantly. The negative correlation is enhanced compared to the system without blowing, suggesting that the overlapping of positive- and negative-signed streamwise vortices is increased in the upward motion. In the downward motion (figure 22*c*), the streamwise length scales of $R_{\omega_x \omega_x}$ are slightly decreased compared with the no-blowing condition.

Contour plots of the two-point cross-correlation coefficient between the streamwise vorticity ω_x' and the stretching term $(\omega_x \partial u/\partial x)'$ are shown in figure 23. For no blowing, the correlation shows an elongated positive region in the streamwise direction, similar to $R_{\omega_x \omega_x}$. However, $R_{\omega_x \mathrm{ST}}$ does not show negative regions. The inclination angle of $R_{\omega_x \mathrm{ST}}$ in the (x, y)-plane is about 6.4°, which is slightly smaller than that of $R_{\omega_x \omega_x}$. Ong & Wallace (1998) showed by examining the quadrants of ω_x and $\omega_x \partial u/\partial x$ that Q1 ($\omega_x > 0$, $\omega_x \partial u/\partial x > 0$) and Q3 ($\omega_x < 0$, $\omega_x \partial u/\partial x < 0$) are dominant in the rate of increase of streamwise vorticity fluctuations. This suggests that $\partial u/\partial x > 0$ is important in the stretching term $\omega_x^2 \partial u/\partial x$. Jeong *et al.* (1997) reported that positive $\partial u/\partial x$ occurs at the centre of the streamwise vortical structure regardless of its sign, since ejection (sweep) occurs upstream (downstream) of the streamwise vortex. This

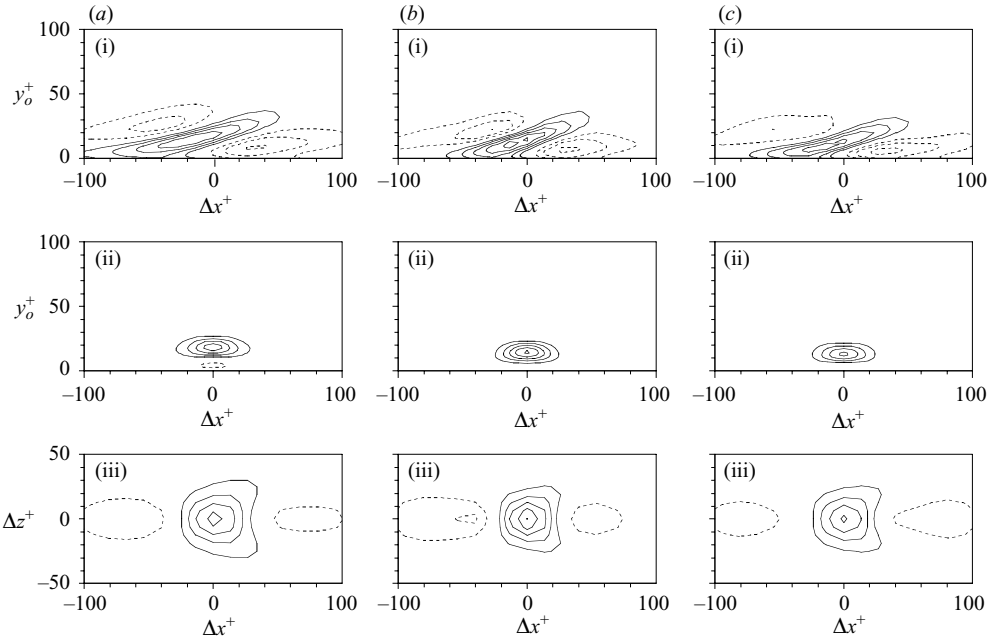

FIGURE 24. Contours of $R_{\omega_x \mathrm{TT1}}(\Delta x, y, \Delta z)$ for $Re_{\theta,in} = 670$. (*a*) NB ($A^+ = 0$); (*b*) upward motion; (*c*) downward motion.

is consistent with the present observation that the region of positive $R_{\omega_x \mathrm{ST}}$ is located inside the region of the streamwise vortical structure. For periodic blowing, as shown in figures 23(*b*) and 23(*c*), the negative correlation which is not detected for no blowing, is observed above (below) the streamwise vortex in the upward (downward) motion, respectively. It is clearly seen that in the downward motion (figure 23*c*), $R_{\omega_x \mathrm{ST}}$ is significantly increased compared to both the upward motion and the no-blowing condition, indicating that the downward motion enhances the stretching term due to $\partial u/\partial x > 0$ as the flow spreads out. This is consistent with the enhancement of the phase-averaged stretching term in the downward motion in figure 21(*d*).

Figure 24 shows the contour plots of the two-point cross-correlation coefficient between the streamwise vorticity ω_x' and the tilting term $(-(\partial w/\partial x)(\partial u/\partial y))'$. The correlation $R_{\omega_x \mathrm{TT1}}$ behaves differently from $R_{\omega_x \mathrm{ST}}$. Specifically, for no blowing (figure 24*a*), a region of positive correlation is located between regions of negative correlation in the streamwise direction, with the maximum correlation being observed at $\Delta x^+ = -17$ (i.e. slightly upstream of the reference position). The inclination angle of the region of positive $R_{\omega_x \mathrm{TT1}}$ in the (x, y)-plane is about 16.5°, which is twice that of $R_{\omega_x \omega_x}$. Brooke & Hanratty (1993) investigated the evolution of the conditional averaged streamwise vortices by using $(-\partial w/\partial x)(\partial u/\partial y)$ as a criterion for conditional averaging. They showed that conditionally sampling for positive $(-\partial w/\partial x)(\partial u/\partial y)$ yields a positive streamwise vortex in the downstream. In the present study, in the region $y^+ < 10$, the correlation has a positive value for $\Delta x^+ < 0$ and a negative value for $\Delta x^+ > 0$ (figure 24*a*). The positive (negative) $(-\partial w/\partial x)(\partial u/\partial y)$ indicates that the positive streamwise vortex exists in the downstream (upstream). In the upward motion (figure 24*b*), the streamwise extent of the positive $R_{\omega_x \mathrm{TT1}}$ in the region $y^+ < 10$ is decreased and is shifted to less upstream as compared with that of no blowing. Similar behaviour is observed in the downward motion (figure 24*c*). The correlation

$R_{\omega_x \mathrm{TT1}}$ did not show any significant difference on going from the upward to the downward motion, whereas $R_{\omega_x \mathrm{ST}}$ changed in magnitude and in length scale.

5. Conclusions

A detailed numerical analysis has been performed to elucidate the effects of localized periodic blowing on a turbulent boundary layer. Time-periodic blowing was applied through a spanwise slot by varying the wall-normal velocity in a cyclic manner from 0 to $2A^+$. The time-periodic blowing was applied with frequencies in the range $0 \leqslant f^+ \leqslant 0.08$ at a fixed blowing amplitude of $A^+ = 0.5$. Direct numerical simulations of a spatially evolving turbulent boundary layer were carried out for two Reynolds numbers, $Re_{\theta,in} = 300$ and 670. The results for the steady blowing showed that the local blowing enhanced both the streamwise vortices and the energy redistribution in the system. For the systems with $Re_{\theta,in} = 300$ and 670, the flow variables showed almost the same response for the same σ^+, which implies that σ^+ can be used as a general parameter for local blowing on a low-Reynolds-number turbulent boundary layer. For the periodic blowing, application of blowing at a frequency of $f^+ = 0.035$ was found to give the maximum increases in Reynolds shear stress, streamwise vorticity fluctuations and energy redistribution. The time-averaged streamwise velocity was invariant with the blowing frequency. However, the blowing frequency effect was clearly observed in the phase-averaged velocities; specifically, as the blowing frequency increased, $\tilde{u}_{rms}$ and $\tilde{v}_{rms}$ decreased. Application of periodic blowing caused the velocity fluctuations and Reynolds shear stress to increase compared to the no-blowing case. The increase of u'_{rms} for $f^+ = 0.035$ is smaller than those for other frequencies, whereas the increases of v'_{rms}, w'_{rms} and $-\overline{u'v'}$ for $f^+ = 0.035$ are larger than those for other frequencies. Reynolds stress budget analysis revealed that the effective blowing frequency ($f^+ = 0.035$) induces the greatest enhancement of the pressure–strain term. Analysis of the phase-averaged streamwise vorticity and its stretching and tilting terms showed that the 'downward' motion of the phase-averaged velocity enhanced the stretching term and the 'upward' motion lifted the strengthened layer of ω'_x, thereby causing the interaction between the strengthened layer of ω'_x and the wall to become weaker, and the lifted vortices to become stronger. The correlation coefficients $R_{\omega_x\omega_x}$, $R_{\omega_x \mathrm{ST}}$ and $R_{\omega_x \mathrm{TT1}}$ were calculated to quantitatively describe the response of the turbulent coherent structures to the periodic blowing. In the upward motion, the streamwise length scale of $R_{\omega_x\omega_x}$ decreased significantly. In the downward motion, $R_{\omega_x \mathrm{ST}}$ increased significantly compared with both the 'upward' motion and the no-blowing case, suggesting that the stretching term is the dominant contributing term in the periodic blowing-induced increase in streamwise vorticity. The correlation $R_{\omega_x \mathrm{ST}}$ changed in magnitude and in length scale from the upward to the downward motion, whereas $R_{\omega_x \mathrm{TT1}}$ did not show any significant difference.

The authors would like to acknowledge the support from KISTI (Korea Institute of Science and Technology Information) under 'The Sixth Strategic Supercomputing Support Program.' The use of the computing system of the Supercomputing Centre is also greatly appreciated.

REFERENCES

Antonia, R. A., Zhu, Y. & Sokolov, M. 1995 Effect of concentrated wall suction on a turbulent boundary layer. *Phys. Fluids* **7**, 2465–2474.

Brooke, J. W. & Hanratty, T. H. 1993 Origin of turbulence-producing eddies in a channel flow. *Phys. Fluids* **5**, 1011–1022.

Choi, H., Moin, P. & Kim, J. 1993 Direct numerical simulation of turbulent flow over riblets. *J. Fluid Mech.* **255**, 503–539.

Choi, J.-I., Xu, C.-X. & Sung, H. J. 2002 Drag reduction by spanwise wall oscillations in wall-bounded turbulent flows. *AIAA J.* **40**, 842–850.

Choi, K.-S., Yang, X., Clayton, B. R., Glover, E. J., Atlar, M., Semenov, B. N. & Kulik, V. M. 1997 Turbulent drag reduction using compliant surfaces. *Proc. R. Soc. Lond.* A **453**, 2229–2240.

Chung, Y. M. & Sung, H. J. 2001 Initial relaxation of spatially evolving turbulent channel flow with blowing and suction. *AIAA J.* **39**, 2091–2099.

Chung, Y. M., Sung, H. J. & Krogstad, P.-Å. 2002 Modulation of near-wall turbulence structure with wall blowing and suction. *AIAA J.* **40**, 1529–1535.

Gad-el-Hak, M. 2000 *Flow Control: Passive, Active, and Reactive Flow Management*. Cambridge University Press.

Hammond, E. P., Bewley, T. R. & Moin, P. 1998 Observed mechanisms for turbulence attenuation and enhancement in opposition-controlled wall-bounded flows. *Phys. Fluids* **10**, 2421–2423.

Jeong, J., Hussain, W., Schoppa, W. & Kim, J. 1997 Coherent structures near the wall in a turbulent channel flow.*J. Fluid Mech.* **332**, 185–214.

Kim, C., Jeon, W.-P., Park, J. & Choi, H. 2003*a* Effects of a localized time-periodic wall motion on a turbulent boundary layer flow. *Phys. Fluids* **15**, 2142–2145.

Kim, J., Kim, K. & Sung, H. J. 2003*b* Wall pressure fluctuations in a turbulent boundary layer after blowing or suction. *AIAA J.* **41**, 1697–1704.

Kim, J., Moin, P. & Moser, R. 1987 Turbulence statistics in fully developed channel flow a low Reynolds number. *J. Fluid Mech.* **177**, 133–166.

Kim, K. 2005 Effects of local forcing on a turbulent boundary layer. PhD thesis, Korea Advanced Institute of Science and Technology.

Kim, K., Baek, S.-J. & Sung, H. J. 2002*a* An implicit velocity decoupling procedure for the incompressible Navier–Stokes equations. *Intl J. Numer. Meth. Fluids* **38**, 125–138.

Kim, K. & Sung, H. J. 2003 Effects of periodic blowing from a spanwise slot on a turbulent boundary layer. *AIAA J.* **41**, 1916–1924.

Kim, K., Sung, H. J. & Chung, M. K. 2002*b* Assessment of local blowing and suction in a turbulent boundary layer. *AIAA J.* **40**, 175–177.

Kravchenko, A. G., Choi, H. & Moin, P. 1993 On the relation of near-wall streamwise vortices to wall skin friction in turbulent boundary layers. *Phys. Fluids* **5**, 3307–3309.

Krogstad, P.-Å. & Kourakine, A. 2000 Some effects of localized injection on the turbulence structure in a boundary layer. *Phys. Fluids* **12**, 2990–2999.

Lund, T. S., Wu, X. & Squires, K. D. 1998 Generation of turbulent inflow data for spatially-developing boundary layer simulation. *J. Comput. Phys.* **140**, 233–258.

Na, Y. & Moin, P. 1996 Direct numerical simulation of turbulent boundary layers with adverse pressure gradient and separation. *Rep.* **TF-68**. Department of Mechanical Engineering, Stanford University.

Na, Y. & Moin, P. 1998 The structure of wall-pressure fluctuations in turbulent boundary layers with adverse pressure gradient and separation. *J. Fluid Mech.* **377**, 347–373.

Ong, L. & Wallace, J. M. 1998 Joint probability density analysis of the structure and dynamics of the vorticity field of a turbulent boundary layer. *J. Fluid Mech.* **367**, 291–328.

Park, J. & Choi, H. 1999 Effects of uniform blowing or suction from a spanwise slot on a turbulent boundary layer. *Phys. Fluids* **11**, 3095–3105.

Park, S.-H., Lee, I. & Sung, H. J. 2001 Effect of local forcing on a turbulent boundary layer. *Exps. Fluids* **31**, 384–393.

Park, Y.-S., Park, S.-H. & Sung, H. J. 2003 Measurement of local forcing on a turbulent boundary layer using PIV. *Exps. Fluids* **34**, 697–707.

Rhee, G. H. & Sung, H. J. 2001 Numerical prediction of locally-forced turbulent boundary layer. *Intl J. Heat Fluid Flow* **22**, 624–632.

Robinson, S. K. 1991 Coherent motions in the turbulent boundary layer. *Annu. Rev. Fluid Mech.* **23**, 601–639.

Sano, M. & Hirayama, N. 1985 Turbulent boundary layer with injection and suction through a slit. *Bull. JSME* **28**, 807–814.

Senda, M., Kawaguchi, Y., Suzuki, K. & Sato, T. 1981 Study on a turbulent boundary layer with injection. *Bull. JSME* **24**, 1748–1755.

Spalart, P. R. 1988 Direct simulation of a turbulent boundary layer up to $Re_\theta = 1410$. *J. Fluid Mech.* **187**, 61–98.

Sumitani, Y. & Kasagi, N. 1995 Direct numerical simulation of turbulent transport with uniform wall injection and suction. *AIAA J.* **33**, 1220–1228.

Tardu, S. 1998 Near wall turbulence control by local time periodic blowing. *Exp. Thermal Fluid Sci.* **16**, 41–53.

Tardu, S. F. 2001 Active control of near-wall turbulence by local oscillating blowing. *J. Fluid Mech.* **439**, 217–253.